https://doi.org/10.1093/plphys/kiad439 PLANT PHYSIOLOGY 2023: 193: 1797–1815

Plant Physiology®

Research Article

# Three consecutive cytosolic glycolysis enzymes modulate autophagic flux

Du-Hwa Lee [1,2,*,†,‡] Ilyeong Choi [2,†] Seung Jun Park,[2] Sumin Kim [2] Min-Soo Choi [1] Ho-Seok Lee [3,4] and Hyun-Sook Pai [2,*]

1 Gregor Mendel Institute (GMI), Austrian Academy of Sciences, Vienna BioCenter (VBC), Dr. Bohr-Gasse 3, 1030 Vienna, Austria
2 Department of Systems Biology, Yonsei University, Seoul 03722, Korea
3 Department of Biology, Kyung Hee University, Seoul 02447, Korea
4 Center for Genome Engineering, Institute for Basic Science, Daejeon 34126, Korea

*Author for correspondence: hspai@yonsei.ac.kr (H-S.P.), duhwa.lee@gmi.oeaw.ac.at (D-H.L.)
†D.-H.L. and I.C. contributed equally to this work.
‡Current address: Institute of Organic Chemistry, BOKU-University of Natural Resources and Life Sciences, Muthgasse 18, 1190 Vienna, Austria.
The author responsible for distribution of materials integral to the findings presented in this article in accordance with the policy described in the Instructions for Authors (https://academic.oup.com/plphys/pages/General-Instructions) is Du-Hwa Lee.

## Abstract

Autophagy serves as an important recycling route for the growth and survival of eukaryotic organisms in nutrient-deficient conditions. Since starvation induces massive changes in the metabolic flux that are coordinated by key metabolic enzymes, specific processing steps of autophagy may be linked with metabolic flux-monitoring enzymes. We attempted to identify carbon metabolic genes that modulate autophagy using VIGS screening of 45 glycolysis- and Calvin–Benson cycle-related genes in Arabidopsis (*Arabidopsis thaliana*). Here, we report that three consecutive triose-phosphate-processing enzymes involved in cytosolic glycolysis, triose-phosphate-isomerase (TPI), glyceraldehyde-3-phosphate dehydrogenase (GAPC), and phosphoglycerate kinase (PGK), designated TGP, negatively regulate autophagy. Depletion of TGP enzymes causes spontaneous autophagy induction and increases AUTOPHAGY-RELATED 1 (ATG1) kinase activity. TGP enzymes interact with ATG101, a regulatory component of the ATG1 kinase complex. Spontaneous autophagy induction and abnormal growth under insufficient sugar in TGP mutants are suppressed by crossing with the *atg101* mutant. Considering that triose-phosphates are photosynthates transported to the cytosol from active chloroplasts, the TGP enzymes would be strategically positioned to monitor the flow of photosynthetic sugars and modulate autophagy accordingly. Collectively, these results suggest that TGP enzymes negatively control autophagy acting upstream of the ATG1 complex, which is critical for seedling development.

## Introduction

Macroautophagy (hereafter autophagy) is a conserved catabolic process in eukaryotic cells for self-recycling through the degradation of cellular components. Autophagy is activated under starvation conditions. Eukaryotic cells employ AUTOPHAGY-RELATED (ATG) proteins for autophagic processes, from phagophore formation to fusion between autophagosomes and the lysosome or vacuole. Processing and lipidation [phosphatidylethanolamine (PE) conjugation] of ATG8 is the most fundamental step in autophagy (Thompson et al. 2005; Chung et al. 2010). Autophagic flux, which indicates cellular autophagic activity, can be assessed by the lipidation state of ATG8 (Mizushima and Yoshimori 2007; Loos et al. 2014). In the past decade, numerous studies in mammals using sophisticated methods have shown that an autophagic flux is tightly regulated

Received November 03, 2022. Accepted June 19, 2023. Advance access publication August 4, 2023


Open Access

by the mammalian Target Of Rapamycin (mTOR) and AMP-activated protein kinase pathways (Russell et al. 2014). Recent studies have suggested that the ATG1 kinase complex serves as a converging point of multiple upstream signaling pathways for the regulation of autophagic flux in Arabidopsis (*Arabidopsis thaliana*), as observed in mammals and yeast (Mizushima et al. 2010; Chen et al. 2017; Huang et al. 2019). The ATG1 kinase complex consists of ATG1 kinase, scaffold protein ATG11, regulatory subunit ATG13, and ATG101 (Suttangkakul et al. 2011; Zhuang et al. 2018). Except that in ATG101, loss-of-function mutations in the components of the ATG1 kinase complex have been studied, and the results suggested that the ATG1 kinase activity is required for autophagic body deposition under starvation conditions (Suttangkakul et al. 2011; Li et al. 2014; Huang et al. 2019). Upon nutrient starvation, the phosphorylation status of ATG1 and ATG13 can be altered by the activity of evolutionarily conserved central metabolic regulatory kinases, Target of Rapamycin (TOR), and SNF-related kinase1 (SnRK1). ATG1 kinase controls the initiation and growth of autophagosomes, and phosphorylation/dephosphorylation of the ATG1 complex controls the ATG1 activity (Suttangkakul et al. 2011; Chen et al. 2017). Collectively, these findings suggest that the upstream signaling pathways of plant autophagy and the possible regulatory mechanisms of the ATG1 complex depend on nutrient availability. However, the details are still unclear about how autophagic flux is regulated by nutrient availability in plants.

Glycolysis is an ancient metabolic pathway present in all prokaryotes and eukaryotes. Glycolysis produces pyruvate for the tricarboxylic acid cycle, ATP, reduced electron carriers, and intermediates as precursors for diverse metabolic pathways (Plaxton 1996). As plant glycolysis occurs separately in the cytosol and plastids, more isoforms of glycolytic enzymes are present in plants than in other eukaryotes (Plaxton 1996; Rosa-Tellez et al. 2018). Several isoforms of plastidial glycolytic enzymes, such as triose phosphate isomerase (TPI), glyceraldehyde-3-phosphate dehydrogenase (GAPDH), and phosphoglycerate kinase (PGK), are also utilized in the Calvin–Benson cycle. Cytosolic and plastidial isoforms catalyze the same substrate in the cytosol and plastid, respectively. TPI catalyzes the reversible interconversion of dihydroxyacetone phosphate (DHAP) and glyceraldehyde-3-phosphate (GAP), thereby enabling DHAP to enter glycolysis (Chen and Thelen 2010). GAPDH catalyzes the reversible phosphorylation of GAP to 1,3-bisphosphoglycerate (1,3-BPG) in the presence of inorganic phosphate ($P_i$) and nicotinamide adenine dinucleotide ($NAD^+$) (Reis et al. 2013). PGK catalyzes reversible phosphoryl transfer from 1,3-BPG to ADP to produce 3-phosphoglycerate (3-PG) and ATP, the first step for ATP generation during glycolysis (Rosa-Tellez et al. 2018). The triose phosphates produced by photosynthesis are translocated to the cytosol to enter the glycolysis and sucrose biosynthesis pathways for energy production and transportation to other body parts, respectively. Thus, these series of triose-processing enzymes play an important role in carbon metabolism by connecting photosynthesis with cytosolic glycolysis and sucrose biosynthesis.

Recent studies have suggested that several glycolytic enzymes have noncanonical functions in addition to metabolic functions. For example, mammalian aldolase (ALDO) regulates AMP-activated protein kinase (AMPK) activity to sense glucose availability (Zhang et al. 2017). PGK1 acts as a protein kinase for phosphorylation of Beclin1 to regulate autophagy (Qian et al. 2017). There are also examples of "moonlighting" behaviors of several glycolytic enzymes in plants. Hexokinase 1 (HXK1), an isoform of the first enzyme in the glycolysis pathway, acts as a glucose sensor and modulates the transcription of sucrose-responsive genes (Cho et al. 2006). Cytosolic GAPDH1 and 2 (GAPCs) respond to heat stress by translocating into the nucleus and increasing the expression of heat-inducible genes (Kim et al. 2020). Furthermore, there is a recent report that the stability of several cytosolic glycolytic enzymes, including ALDO, TPI, and PGK, is modulated by autophagy (Li et al. 2022). Autophagy also contributes to adjusting metabolic homeostasis in plants, indicating a close relationship between autophagy and metabolism (Izumi et al. 2013; Masclaux-Daubresse et al. 2014; Avin-Wittenberg et al. 2015). Finally, cytosolic GAPCs repress the induction of autophagy, caused by reactive oxygen species in *Nicotiana benthamiana* and *Arabidopsis* (Han et al. 2015; Henry et al. 2015). Collectively, these results suggest the diversity and importance of noncanonical functions of glycolysis enzymes and their possible involvement in the regulation of autophagy (Michaeli et al. 2016).

In this study, we discovered the noncanonical functions of three specific glycolytic enzymes in the control of autophagy. The three glycolytic enzymes are cytosolic triose phosphate isomerase (CyTPI), cytosolic phosphorylating glyceraldehyde-3-phosphate dehydrogenase 1 and 2 (GAPCs), and phosphoglycerate kinase 3 (PGK3), designated TGP enzymes. The TGP enzymes catalyze the three consecutive steps in the cytosolic glycolysis pathway, which is closely connected to photosynthesis through the import of DHAP, GAP, and 3-PG from active chloroplasts (Lee et al. 2017b). We performed virus-induced gene silencing (VIGS) screening of carbon metabolic genes. The subsequent analyses suggested that the TGP enzymes negatively regulate autophagy through modulation of ATG1 kinase activity. Considering that plants mainly produce organic carbon compounds via photosynthesis, the noncanonical functions of these glycolytic enzymes may provide a novel strategy to coordinate the autophagic activity with carbon availability.

## Results

### VIGS screening to identify glycolytic enzymes that modulate autophagy

We performed VIGS screening using an *Arabidopsis* autophagy reporter line (35Sp:GFP-ATG8a) to identify negative autophagic regulators of glycolysis enzymes by monitoring the

autophagic flux. Since the TOR kinase complex, which consists of TOR, LST8, and RAPTOR, is a well-characterized negative regulator of autophagy (Liu and Bassham 2010; Pu et al. 2017), we performed VIGS using tobacco rattle virus (TRV) amplicon with *TOR*, *LST8*, and *RAPTOR* genes as proof of concept. Silencing of each TOR complex gene resulted in growth retardation and premature senescence, most by *TOR* silencing (Supplemental Fig. S1A). Silencing of the TOR complex genes resulted in the spontaneous formation of GFP-ATG8a puncta, approximately five times higher than that in the TRV2-myc control, suggesting that VIGS is a reliable tool to identify negative autophagic regulators (Supplemental Fig. S1, B and C).

We launched VIGS screening of 45 genes encoding glycolytic enzymes in *Arabidopsis* (Supplemental Fig. S2; *written in red*) and monitored GFP-ATG8a puncta levels after silencing of each gene. We observed leaf epidermal cells of the VIGS plants using fluorescence microscopy and ranked them by GFP-ATG8a puncta numbers (Fig. 1A). After VIGS of 45 genes, only four genes encoding TGP enzymes in the cytosolic glycolysis pathway showed statistically significant GFP-ATG8a puncta formation compared to the negative control (TRV-myc) (Fig. 1, A and B). TGP enzymes include cytosolic triose phosphate isomerase (CyTPI), cytosolic phosphorylating glyceraldehyde-3-phosphate dehydrogenase 1 and 2 (GAPC1 and 2), and phosphoglycerate kinase 3 (PGK3). We performed VIGS on selected genes for confirmation of screening results. Silencing of *CyTPI* and *PGK3* and cosilencing of *GAPC1* and *GAPC2* (*GAPCs*) resulted in retarded plant growth (Supplemental Fig. S3A). The silencing efficiency of each VIGS sample was determined using reverse transcription quantitative PCR (RT-qPCR) (Supplemental Fig. S3, B and C). The TGP enzymes catalyze the sequential processing of triose phosphates, which are produced by the cytosolic glycolysis pathway as well as by the Calvin–Benson cycle in chloroplasts and transported to the cytosolic pathway (Fig. 1B). Based on the Z-stack projection of confocal microscopy images (Fig. 1C), the number of GFP-ATG8a puncta was quantified (Fig. 1D). Compared with that in the control TRV2-myc, depletion of the cytosolic TGP enzymes (CyTPI, GAPCs, and PGK3) by VIGS caused statistically significant puncta formation, whereas VIGS of the plastidial TGP enzymes (PdTPI, PGK1, and PGK2) or cytosolic cofactor independent phosphoglycerate mutases (iPGAMs) had little effect (Fig. 1, C and D).

The autophagic flux is frequently measured through GFP-ATG8a cleavage, which results in the production of free GFP (Li and Vierstra 2012). Based on immunoblotting with an anti-GFP antibody, free GFP released from GFP-ATG8a was visible in VIGS samples of the TGP enzymes but not in TRV2-myc control or TRV2-Hexokinase 1 (HXK1), suggesting that a deficiency of cytosolic TGP enzymes causes an increase in the autophagic flux (Fig. 1E). Collectively, these data suggest that serial TGP enzymes in the cytosol may act as negative regulators of autophagy in plants.

## Cytosolic TGP enzymes interact with each other

Consecutive enzymes in a metabolic pathway frequently form enzyme subcomplexes for substrate channeling and more efficient regulation. Recent evidence suggests that the glycolytic pathway in mammalian muscle cells consists of several subcomplexes (Menard et al. 2014). To determine whether cytosolic TGP enzymes interact with each other, we performed yeast two-hybrid (Y2H) assays (Supplemental Fig. S4A). GAL4 activating domain (AD)-fused CyTPI and GAL4 promoter binding domain (BD)-fused HXK1, CyTPI, GAPC1, and PGK3 were coexpressed in yeast. Based on yeast growth on selective media, CyTPI interacted with GAPC1 and PGK3, particularly strongly with CyTPI itself (Supplemental Fig. S4A). However, the expression of CyTPI with the BD control or HXK1 did not support positive yeast growth, suggesting no protein interaction. To confirm the interactions between TGP enzymes *in planta*, we performed bimolecular fluorescence complementation (BiFC). $CFP^N$- or $Venus^C$-conjugated CyTPI, GAPC1, PGK3, and control HXK1 were expressed in combination in *N. benthamiana* leaves via agroinfiltration (Fig. 1F, Supplemental Fig. S4B). Split fluorescent proteins, $CFP^N$ and $Venus^C$, reconstitute green fluorescence when their conjugated proteins interact with each other (Gehl et al. 2009). Every combination of CyTPI, GAPC1, and PGK3 produced green fluorescence in the cytosol, but the combination with HXK1 did not produce any fluorescent signal. Collectively, these results suggest interactions between the cytosolic TGP enzymes.

## Cytosolic TGP enzyme mutants show abnormal seedling growth depending on sucrose concentration

To confirm the results of VIGS, we analyzed T-DNA insertion lines for *HXK1*, *CyTPI*, *GAPC1*, *GAPC2*, and *PGK3* (Supplemental Fig. S5) and detected very low or undetectable levels of transcripts using RT-qPCR (Supplemental Fig. S5). Before analyzing the autophagic flux in these mutants, we observed the overall seedling growth in the MS medium containing various sugar concentrations. Interestingly, the cytosolic TGP enzyme mutants *cytpi*, *gapc1/2* (*gapc1-1/gapc2-1* double mutant), *pgk3-1*, and *pgk3-2* all showed similar defects in leaf development near the shoot apical meristem (SAM) under 15 mM sucrose concentration (Fig. 2A, Supplemental Fig. S6). Compared to the wild-type (WT) and *hxk1-3*, these mutants produced leaves with abnormal thickness and shape, which suggested defective cell division and expansion (Fig. 2A). The frequency of developmental abnormalities in the cytosolic TGP enzyme mutants was significantly higher than that in WT and *hxk1-3* mutants; the *cytpi* and *pgk3-2* mutants exhibited particularly high levels of abnormalities (Fig. 2B). However, the frequency of abnormal development in the TGP mutants significantly and progressively decreased under 30 and 60 mM sucrose (Fig. 2B, Supplemental Fig. S6). These findings suggest that the deficiency of cytosolic TGP enzymes causes seedling growth defects depending on sugar concentration.

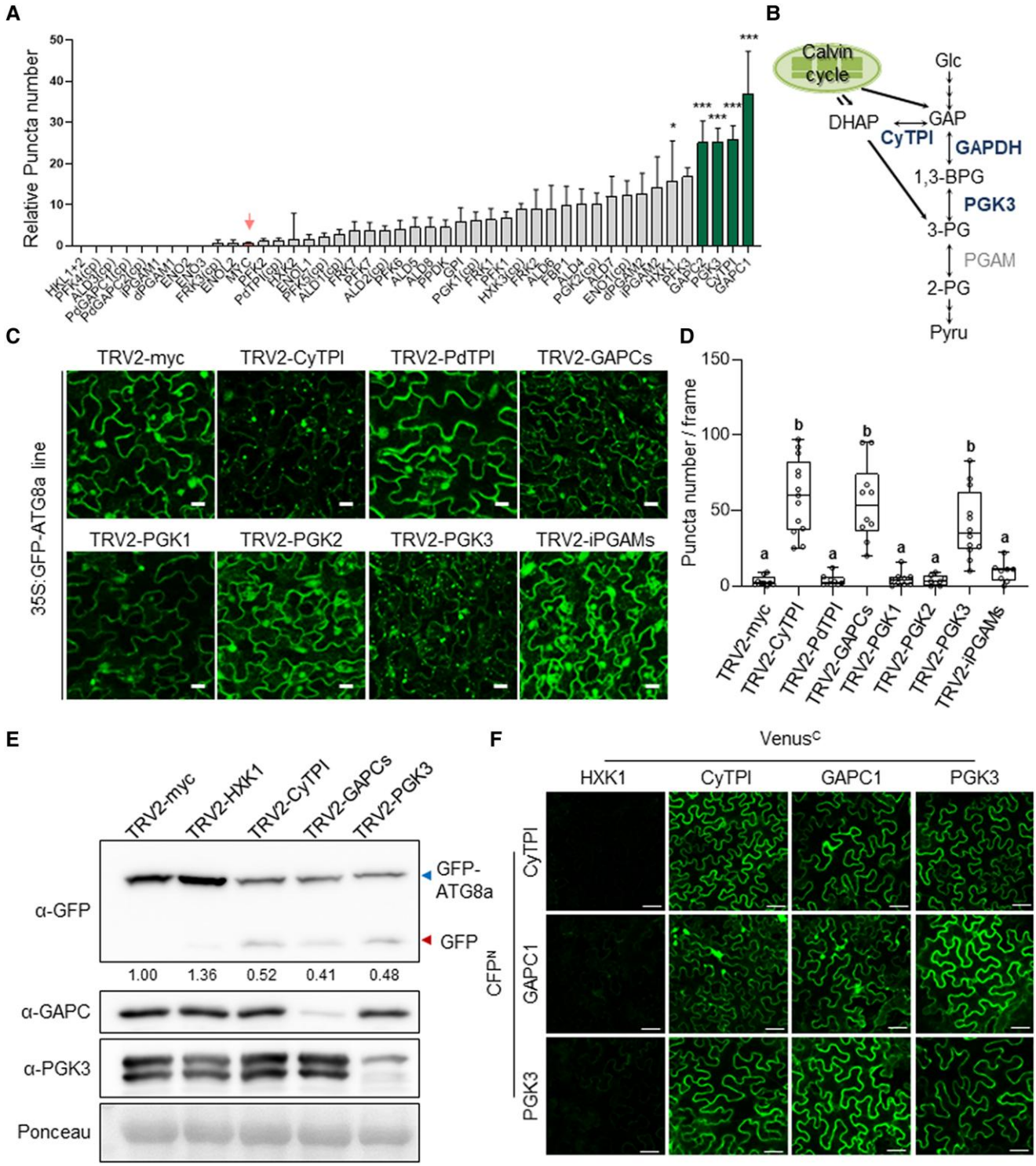


**Figure 1.** Silencing of cytosolic TGP enzyme genes causes increased autophagic flux. **A)** Measurement of relative puncta numbers per frame compared to TRV2-myc in fluorescent microscopic images. Enzymes are ordered from left to right by increasing relative puncta numbers. Error bars represent SE from at least 3 independent observations. Statistical significance is assessed using linear regression analysis compared to TRV2-myc (coefficient *P*-value; *, $P < 0.05$; ***, $P < 0.001$). The *green bars* represent the genes showing statistically significant differences ($P < 0.001$). The *arrow* indicates TRV2-myc, the negative control of VIGS screening. The chloroplast enzymes (including the putative ones) were marked by "(cp)" after enzyme names. **B)** A schematic diagram of a part of the cytosolic glycolysis pathway that shows three enzymes CyTPI, GAPDH, and PGK3 (marked by *boldface*) and metabolites. Transport of triose phosphates GAP, DHAP, and 3-PG from chloroplasts to the cytosol is indicated by *thick lines*. The full glycolysis pathway in the cytosol and the Calvin-Benson cycle in chloroplasts are shown in Supplemental Fig. S2. **C)** Confocal microscopy of

(continued)

## Cytosolic TGP enzyme mutants have higher autophagic flux than wild-type

To examine the autophagic flux in cytosolic TGP enzyme mutants, we observed autophagosomes by following the fluorescence of GFP-ATG8a in WT and glycolytic mutants using confocal microscopy (Fig. 2C). Mesophyll protoplasts were prepared from the WT and mutant plants and transfected with the GFP-ATG8a construct. The protoplasts were then treated with the dimethyl sulfoxide (DMSO) control or Concanamycin A (Con A) for 16 h. Con A blocks the vacuolar degradation of autophagosomes by specifically inhibiting vacuolar ATPase (Dettmer et al. 2006). The average number of GFP-ATG8a puncta in the protoplast was higher in the cytosolic TGP enzyme mutants than in the WT and *hxk1-3* mutants, and the effect was more visible upon Con A treatment (Fig. 2, C to E). Increased puncta numbers following Con A treatment suggested that the formation of excessive puncta in the TGP enzyme mutants was not caused by vesicle trafficking defects. These observations, i.e. the increase in ATG8a-positive puncta formation in the cytosolic TGP enzyme mutants, were consistent with the results of VIGS screening (Fig. 1, C and D).

Immunoblotting of LC3 (mammalian ATG8 homolog) can be easily performed to result in a clear separation of bands for LC3 and its lipidation form. However, in plants, more complex methods—e.g. using membrane-enriched fraction and 6 M urea-gel—have been used to separate ATG8 and ATG8-PE (phosphatidylethanolamine) in immunoblots. To simplify the immunoblotting technique to detect ATG8/ATG8-PE in plants, we modified the procedure, as described in Materials and methods. To test the modified method, we compared the band patterns of ATG8/ATG8-PE between Col-0 and *atg5-1* mutant seedlings (Supplemental Fig. S7A). The modified immunoblotting method clearly detected both ATG8 and ATG8-PE bands for quantification, and the ATG8-PE/ATG8 ratio was lower in *atg5-1* than in Col-0 (Supplemental Fig. S7A). We further tested the modified technique using plants under starvation conditions with increased autophagic flux. 35Sp:GFP-ATG8a and WT seedlings were grown in sugar-free media for 1 day in the dark and then supplied with various concentrations of glucose (0 to 30 mM) for incubation in the dark for 1 day (Supplemental Fig. S7B). Immunoblotting revealed that increasing glucose concentrations progressively increased GFP-ATG8a levels and decreased ATG8-PE/ATG8 ratio (Supplemental Fig. S7, C and D). Notably, both immunoblotting showed conspicuous changes in GFP-ATG8 and ATG8-PE levels upon 5 mM glucose treatment. These results suggest that the modified immunoblotting method is suitable for measuring the ATG8-PE/ATG8 ratio to monitor changes in the autophagic flux. Thus, we examined the ATG8 band patterns using the modified immunoblotting method in the TGP enzyme mutants to confirm the increased autophagic flux in the mutants. Immunoblotting using an anti-ATG8 antibody showed a higher ATG8-PE/ATG8 ratio in cytosolic TGP enzyme mutants than in the WT and *hxk1-3* mutants, not only after dark/starvation (DS) treatment for 2 days (Supplemental Fig. S7E), but also under normal conditions (Fig. 2F). Collectively, these results suggest that the depletion of cytosolic TGP enzymes increases the autophagic flux.

## Cytosolic TGP enzymes interact with ATG101

Upon nutrient starvation, energy signaling pathways such as the TOR and SnRK1 pathways converge on the ATG1 kinase complex to modulate autophagic flux (Chen et al. 2017; Pu et al. 2017). As the autophagic flux is directly related to the ATG1 kinase activity in eukaryotes, we examined the possible interactions of glycolytic enzymes, including cytosolic TGP enzymes, with the regulatory subunits of the ATG1 kinase complex (ATG101, ATG13a, and ATG13b). To determine these interactions, $Venus^N$-fused glycolytic enzymes (HXK1, CyTPI, PdTPI, GAPC1, GAPC2, PGK2, and PGK3) and $Venus^C$-fused ATG101 were coexpressed in *N. benthamiana* leaves for BiFC assays. Confocal microscopy detected fluorescence in the cytosol of leaf epidermal cells expressing CyTPI, GAPC1, GAPC2, and PGK3, along with ATG101, suggesting interactions between ATG101 and these enzymes. Among these positive interactions, large fluorescent foci were observed with CyTPI, GAPC1, and GAPC2 but not with PGK3 (Fig. 3A, *upper*). These BiFC results were confirmed by fusing the constructs with $Venus^N$ or $Venus^C$ in a reverse manner (Fig. 3A, *lower*). Both BiFC experiments consistently showed

**Figure 1.** (Continued)
GFP-ATG8a fluorescence (Z-stack image projection) in leaf epidermal cells after VIGS of the glycolytic enzyme genes at 14 days after infiltration (DAI). TRV2-myc was used as a control for VIGS. Silencing of *CyTPI*, *GAPCs*, and *PGK3* led to spontaneous formation of GFP-ATG8a puncta. VIGS using TRV2:GAPCs and TRV2:iPGAMs constructs caused cosilencing of *GAPC1* and *GAPC2*, and *iPGAM1* and *iPGAM2*, respectively. Scale bar = 10 $\mu$m. **D)** Puncta numbers per frame in the Z-stack of confocal microscopy images. Dots represent puncta numbers of individual observations. The box plot represents the 1st and 3rd quartiles, center line indicates the median, and whiskers include the min and max of the data points. Letters above the boxes (*a* and *b*) indicate the results of one-way ANOVA followed by Tukey's multiple comparison test ($P < 0.05$). **E)** Detection of free-GFP release by autophagic breakdown of the GFP-ATG8a reporter. Total leaf extracts from VIGS plants were subjected to immunoblotting with anti-GFP, anti-GAPC, and anti-PGK3 antibodies. The GFP-ATG8a fusion protein and free-GFP are indicated by *arrowheads*, respectively. The anti-PGK3 antibody generated two protein bands, and the lower bands appeared to represent PGK3 enzyme. Ponceau S-stained rubisco large subunit (rbcL) was used as the loading control. Relative band intensities of GFP-ATG8a are indicated below the anti-GFP image. **F)** BiFC analyses for interactions between glycolytic enzymes. The $CFP^N$-and $Venus^C$-fusion constructs were coexpressed in *N. benthamiana* leaves via agroinfiltration. Leaf epidermal cells were observed by confocal microscopy. Scale bar = 50 $\mu$m.

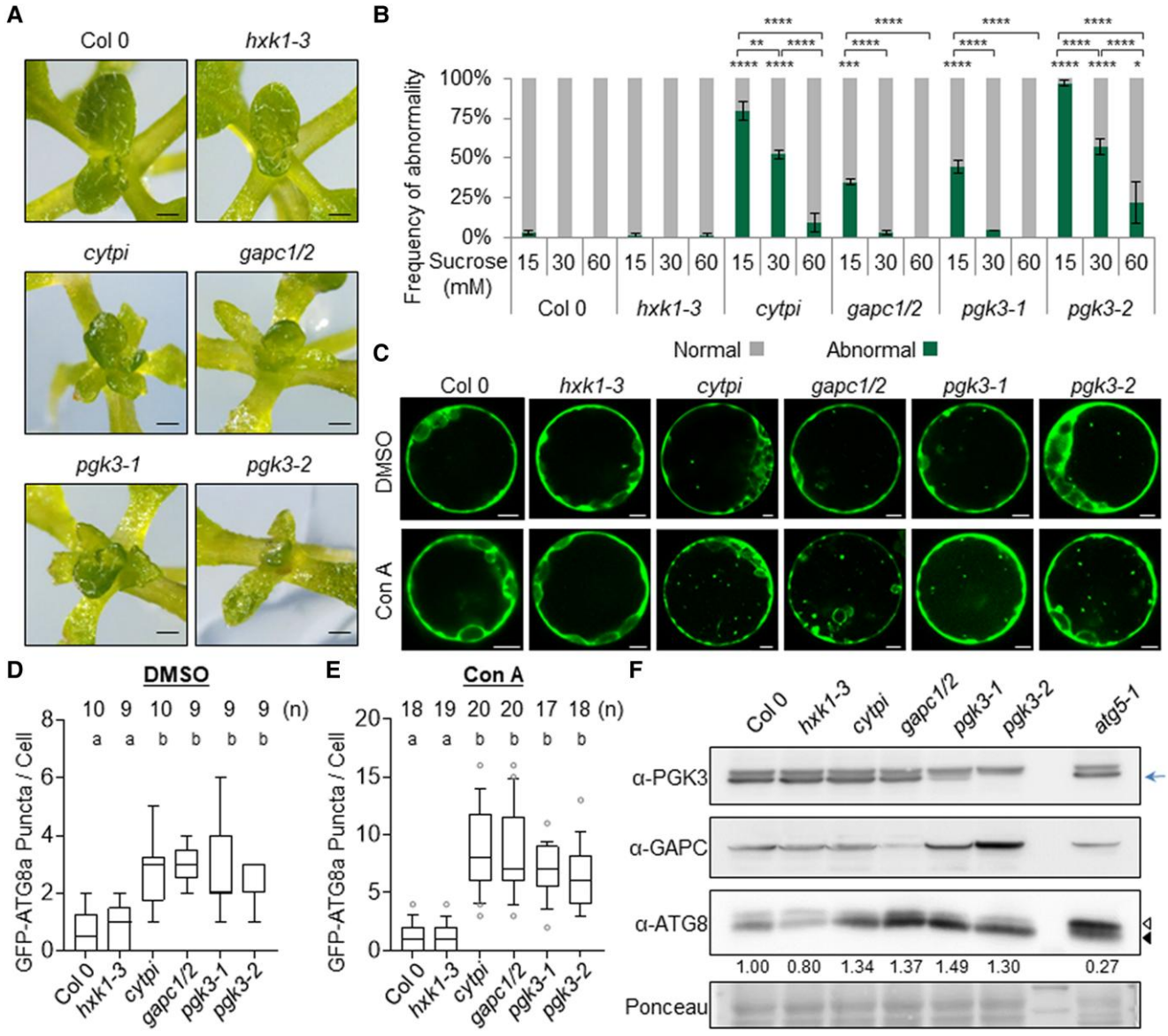


**Figure 2.** The cytosolic TGP enzyme mutants show higher autophagic flux, accompanied by abnormal shoot growth in a sugar-dependent manner. **A)** Representative close-up views of the shoot apical region in the glycolysis mutants grown in 15 mM sucrose. The whole pictures of the seedlings are shown in Supplemental Fig. S6. Emerging abnormal leaves were visible in *cytpi*, *gapc1/2*, *pgk3-1*, and *pgk3-2* mutants. Scale bars = 0.25 mm. **B)** Frequency of abnormal shoot growth in the mutants. The bar graphs show percentages of defective seedlings out of total 20 seedlings in different sucrose concentrations (15, 30, and 60 mM). Error bars represent SE from three biological replications. Statistical significance was assessed using one-way ANOVA followed by Tukey's multiple comparison test (*, $P < 0.05$; **, $P < 0.01$; ***, $P < 0.001$; ****, $P < 0.0001$). The statistical significances compared to WT (Col-0) under the same sucrose concentration are marked at the top of the bars, while other comparisons are indicated by respective *brackets*. **C)** Confocal microscopy of GFP-ATG8a fluorescence (Z-stack image projection) in *Arabidopsis* mesophyll protoplasts of the glycolysis mutants. Leaf protoplasts were transfected with the GFP-ATG8a construct, followed by treatment with DMSO (control) or 1 $\mu$M concanamycin A (Con A). Scale bars = 5 $\mu$m. **D, E)** The GFP-ATG8a puncta in the protoplasts were counted in Z-stacked confocal microscopy images after DMSO (D) or Con A (E) treatment. Puncta numbers per frame are shown in the Z-stack of confocal microscopy images. The box plot represents 1st and 3rd quartiles, center line indicates the median, represented dots are outliers, and whiskers include the 10th to 90th percentile of the data points. The number of biologically independent observations (n) is indicated at the top of the graph. Letters above the boxes (*a–c*) indicate the results of one-way ANOVA followed by Tukey's multiple comparison test ($P < 0.05$). **F)** Immunoblotting for monitoring ATG8-PE/ATG8 patterns in the glycolysis mutants. Twelve-day-old seedlings were incubated in the light in the liquid medium containing 30 mM glucose. Protein extracts were subjected to immunoblotting with anti-PGK3, anti-GAPC, and anti-ATG8 antibodies. The *atg5-1* autophagy mutant was used as the positive control. The ATG8 and ATG8-PE are marked by *open* and *closed arrowheads*, respectively. The PGK3 protein band is marked by the *arrow*. Relative band intensities of ATG8-PE/ATG8 are indicated below the anti-ATG8 image.

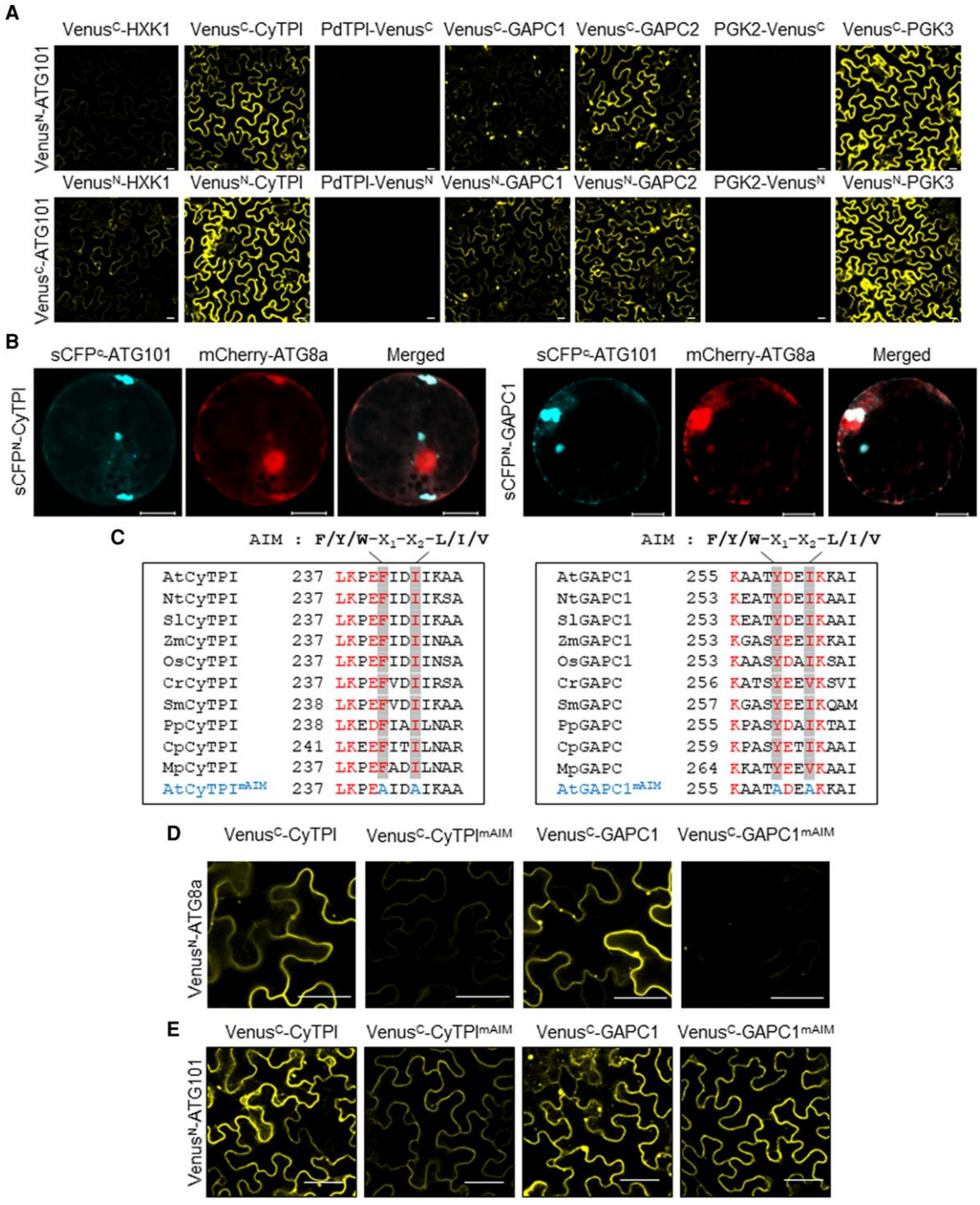


**Figure 3.** The cytosolic TGP enzymes interact with ATG101. **A)** BiFC. Combinations of VENUS$^{N}$- and VENUS$^{C}$-fusion proteins were coexpressed in *N. benthamiana* leaves via agroinfiltration. Venus$^{N}$ and Venus$^{C}$ were fused to the C-terminus of PdTPI and PGK2 that are targeted to chloroplasts. Leaf epidermal cells were observed by confocal microscopy. Scale bars = 20 $\mu$m. **B)** Subcellular colocalization of BiFC fluorescence and mCherry-ATG8a fluorescence in leaf protoplasts. Combinations of CFP$^{N}$- and CFP$^{C}$-fusion proteins were coexpressed with mCherry-ATG8a in *N. benthamiana* leaves via agroinfiltration. Scale bar = 20 $\mu$m. **C)** Conserved AIM sequences in CyTPI and GAPC1 from various plant species. Nt, *Nicotiana tabacum*; Sl, *Solanum lycopersicum*; Zm, *Zea mays*; Os, *Oryza sativa*; Cr, *Ceratopteris richardii* (fern); Sm, *Selaginella moellendorffii* (lycophytes), Pp, *Physcomitrium patens* (bryophytes); Cp, *Ceratodon purpureus* (bryophytes); and Mp, *Marchantia polymorpha* (bryophytes). The consensus sequence of the AIM is shown above the boxes. The first amino acid residue number of the AIM sequence is shown in each protein. Both AtCyTPI$^{mAIM}$ and AtGAPC1$^{mAIM}$ have two amino acid changes to alanine in the conserved AIM sequences as indicated. **D, E)** BiFC analyses to detect interactions of the glycolytic enzymes and their mutants (mAIM) with ATG8a (D) and ATG101 (E). VENUS$^{N}$- and VENUS$^{C}$-fusion proteins were coexpressed in *N. benthamiana* leaves by agroinfiltration. Leaf epidermal cells were observed by confocal microscopy. Scale bar = 20 $\mu$m.

that ATG101 interacts with GAPC1, GAPC2, CyTPI, and PGK3 but not with PdTPI and PGK2 and only weakly with HXK1 (Fig. 3A; Supplemental Fig. S8). In addition, the Venus$^{C}$-fused GAPC1, GAPC2, CyTPI, and PGK3 yielded relatively low levels of fluorescence when coexpressed with Venus$^{N}$-fused ATG13a and ATG13b (Supplemental Fig. S9A). However, the expression of ATG13a or ATG13b in the presence of HXK1, PdTPI, or PGK2 did not generate fluorescence. These results suggest that cytosolic TGP enzymes interact with ATG101 and ATG13 in the cytosol as well as in some foci.

To confirm the interactions between cytosolic TGP enzymes and ATG101, we performed Y2H assays (Supplemental Fig. S9B). AD-fused glycolytic enzymes and BD-fused ATG101 were coexpressed in yeast. Positive yeast growth in selective media suggested interactions between TGP enzymes and ATG101, whereas combinations of HXK1 and ATG101 or AD control and ATG101 did not promote yeast growth, i.e. no protein interaction (Supplemental Fig. S9B), consistent with the results from BiFC (Fig. 3A). Finally, we performed a coimmunoprecipitation experiment to detect protein interactions. HA-tagged glycolytic enzymes (HXK1, CyTPI, GAPC1, and PGK3) and Myc-tagged ATG101 were expressed together in *N. benthamiana* leaves. Myc-ATG101 was immunoprecipitated using an anti-Myc antibody-conjugated resin. Immunoblotting with an anti-HA antibody revealed that HA-CyTPI, HA-GAPC1, and HA-PGK3 coimmunoprecipitated with Myc-ATG101 but not with HA-HXK1 (Supplemental Fig. S9C). Collectively, these results suggest that CyTPI, GAPCs, and PGK3 interact with ATG101 *in vivo* and that those cytosolic TGP enzymes may be involved in autophagic flux regulation.

## CyTPI and GAPC1 require their AIMs to interact with ATG8a and these AIMs are critical for interactions between CyTPI/GAPC1 and ATG101 in large foci

PE-conjugated ATG8 is associated with the autophagosomal membrane (Li and Vierstra 2012). We tested whether the large foci structures observed in the BiFC assays (Fig. 3A) co-localized with ATG8. CFP$^{C}$-ATG101 was coexpressed with CFP$^{N}$-fused CyTPI and GAPC1 and with mCherry-ATG8a in *N. benthamiana* leaves. Protoplasts were then isolated from the infiltrated leaves for observation under a confocal microscope at different excitation wavelengths. Coexpression of CFP$^{C}$-ATG101 with CFP$^{N}$-CyTPI or CFP$^{N}$-GAPC1 caused the formation of fluorescent focilike structures that colocalized with the red fluorescence of mCherry-ATG8a, at least partially (Fig. 3B).

As ATG8-interacting proteins generally contain the ATG8-Interacting motif (AIM), we analyzed the amino acid sequences of CyTPI, GAPC1, GAPC2, PGK3, and ATG101 to search for the consensus sequence of AIM (F/Y/W-$X_1$-$X_2$-L/I/V) (Jia et al. 2019; Marshall et al. 2019). Interestingly, the AIM consensus sequence was found in CyTPI, GAPC1, and GAPC2 but not in PGK3 or ATG101 (Supplemental Fig. S9D), suggesting that ATG8 interactions with these enzymes may play a role in the formation of the large fluorescent foci. Interestingly, the AIM sequences in the CyTPI and GAPC1 proteins were conserved in land plants, including dicots, monocots, ferns, lycophytes, and bryophytes (Fig. 3C). We disrupted AIM sequences in CyTPI$^{mAIM}$ (F241A and I244A) and GAPC1$^{mAIM}$ (Y529A and I262A), respectively. The variants fused with Venus$^{C}$ were coexpressed with Venus$^{N}$-fused ATG8a for BiFC. Confocal microscopy for Venus fluorescence revealed that wild-type CyTPI and GAPC1 interacted with ATG8a in the cytosol and some foci (Fig. 3D). However, BiFC of CyTPI$^{mAIM}$ and GAPC1$^{mAIM}$ variants with ATG8a did not generate fluorescence. We next performed coimmunoprecipitation experiments (Supplemental Fig. S10). GFP-tagged ATG8a was coexpressed with HA-tagged wild-type or mutant enzymes in *N. benthamiana* leaves. HA-tagged enzymes were immunoprecipitated with anti-HA antibody-conjugated resin. Immunoblotting with anti-GFP antibody showed that less amounts of GFP-ATG8a were coimmunoprecipitated with the AIM mutants of CyTPI and GAPC1, compared with the wild-type enzymes. These data suggest that AIM sequences are critical for the interaction between CyTPI/GAPC1 and ATG8 (Fig. 3D, Supplemental Fig. S10). BiFC assays also indicated that wild-type CyTPI and GAPC1 could interact with ATG101 in the cytosol and foci; however, their variants containing the mAIM sequences interacted with ATG101 only in the cytosol (Fig. 3E). Collectively, these results suggest that CyTPI and GAPC1 require their AIMs to interact with ATG8a and that the AIMs are also critical for interactions between CyTPI/GAPC1 and ATG101 in large foci.

## Loss-of-function mutation of *ATG101* results in plant phenotypes similar to those of other ATG1 kinase complex subunit mutations

The ATG1 complex, including the ULK1/2 kinase complex homolog in mammals, regulates the autophagic flux during nutrient starvation (Russell et al. 2013; Huang et al. 2019). The functions of *Arabidopsis* ATG1 kinase complex components in autophagic processes have been characterized, except for those of ATG101. The *atg11* single mutant, *atg13a/atg13b* double mutant, and *atg1abct* quadruple mutant showed typical autophagy-deficient phenotypes, such as hypersensitivity to nitrogen or carbon starvation and premature leaf senescence under short-day conditions (Suttangkakul et al. 2011; Li et al. 2014; Huang et al. 2019). We obtained a mutant line with a T-DNA insertion in the 3rd intron of *ATG101*, designated as *atg101-1*, which has reduced *ATG101* transcript levels than WT plants (Supplemental Fig. S11). We next generated two independent *atg101-1* complementation lines, designated *atg101-1* C-13 and *atg101-1* C-14, with a construct containing the *YFP-ATG101* gene under the control of its own promoter (*ATG101p:YFP-ATG101*).

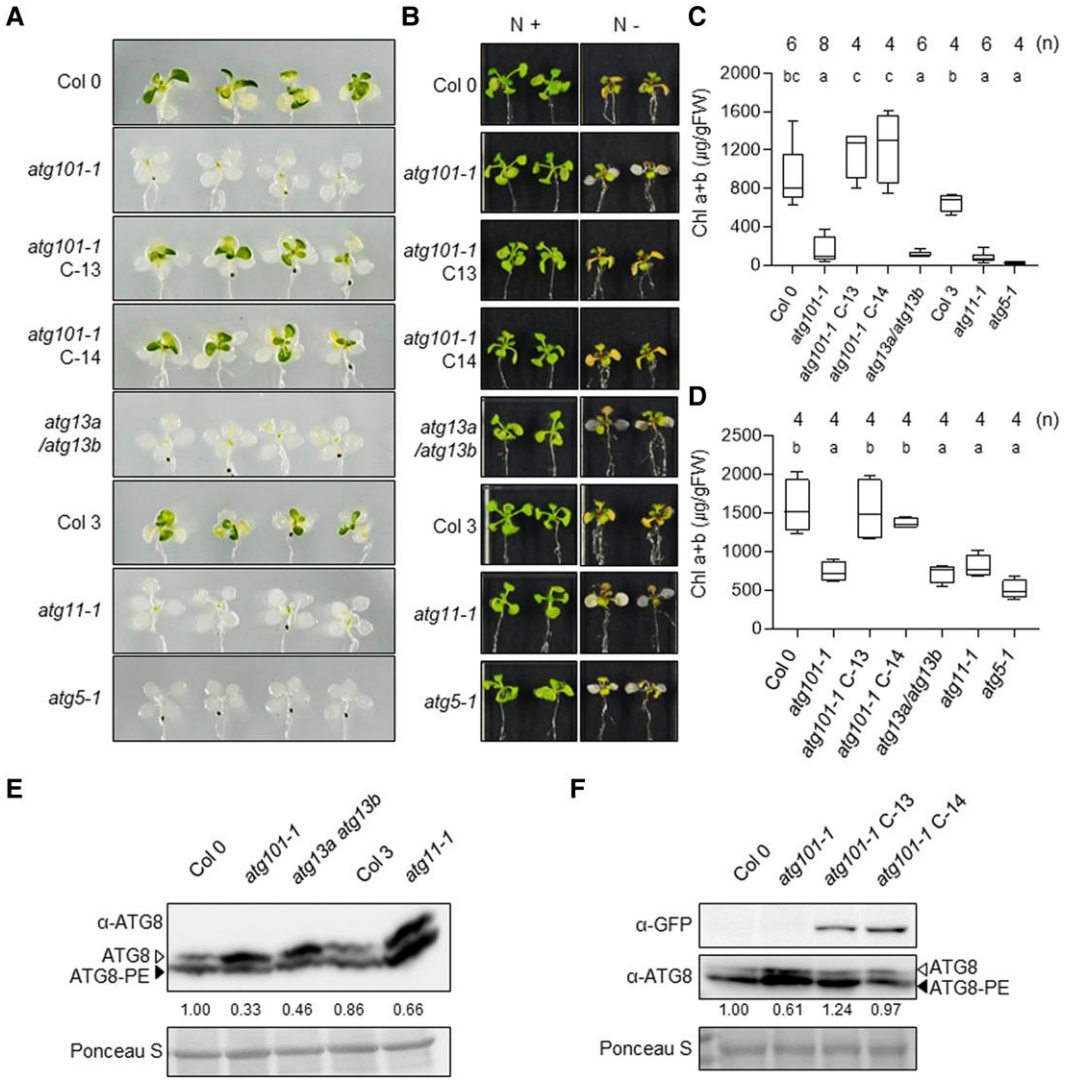


**Figure 4.** The *atg101-1* mutant shows the typical autophagy mutant phenotype and decreased autophagic flux. **A)** Carbon starvation phenotypes of the ATG1 complex mutants and their complementation lines. Twelve-day-old seedlings were transferred to a fresh liquid medium lacking glucose and incubated in the dark for 5 days. Subsequently, the seedlings were supplied with 30 mM glucose and grown in the light for 5 days. The *atg101-1* C-13 and C-14 are two complementation lines of the *atg101-1* mutant, expressing *ATG101p:YFP-ATG101*. The *atg5-1* autophagy mutant was used as the positive control. **B)** Nitrogen starvation phenotype of ATG1 complex mutants. Ten-day-old seedlings were transferred to media with nitrogen (N +) or without nitrogen source (N-) and incubated for 5 days in the light. **C, D)** Total chlorophyll contents in the seedlings shown in (A) and (B). The box plots represent the 1st and 3rd quartiles, centerline indicates median, and whiskers include the 10th to 90th percentile of the data points. The number of biologically independent observations (*n*) is marked on the top of the graph. Letters above the boxes (*a*–*c*) indicate the results of one-way ANOVA followed by Tukey's multiple comparison test ($P < 0.05$). **E, F)** Immunoblotting for monitoring ATG8-PE/ATG8 patterns in the ATG1 complex mutants (E) and the *atg101* complementation line (F). Twelve-day-old seedlings were subjected into immunoblotting with anti-ATG8 antibody. The ATG8 and ATG8-PE are marked by *open* and *closed arrowheads*, respectively. The anti-YFP antibody detected the expression of YFP-ATG101 in the atg101 C-13 and C-14 lines. Ponceau S-stained rubisco large subunit (rbcL) was used as the loading control. Relative band intensities of ATG8-PE/ATG8 are indicated below the anti-ATG8 image.

We performed a carbon-starvation recovery experiment to examine the phenotypes of *atg101-1* mutant and its complementation lines (C-13 and C-14) compared to those of the WT. The WT seedlings (Col-0 and Col-3) generated green leaves by recovering from carbon-starvation, whereas *atg101-1*, *atg13a/atg13b*, *atg11-1*, and *atg5-1* mutants did not produce green leaves (Fig. 4A). Both C-13 and C-14 complementation lines recovered similar green leaves as WTs, suggesting that the *atg101-1* mutant phenotype was rescued by the expression of the *YFP-ATG101* gene (Fig. 4A). The total chlorophyll content was remarkably different between these seedlings, which perfectly matched the visible phenotypes (Fig. 4, A and C). We further examined plant phenotypes in nitrogen-rich (N+) or nitrogen-deficient (N−) media (Fig. 4B). All seedlings were severely affected by nitrogen deficiency, but *atg101-1*, *atg13a/atg13b*, *atg11-1*, and *atg5-1*

mutants contained much lower amounts of chlorophyll than the WT and complementation lines, suggesting more severe defects in autophagy mutants (Fig. 4, B and D).

Next, we analyzed the autophagic flux via immunoblotting to visualize the ATG8-PE and free-ATG8 forms. Immunoblotting using an anti-ATG8 antibody showed that the free-ATG8 form (*closed arrowhead*) was more abundant in the *atg101-1* mutant than in the WT, as similarly observed in *atg13a/atg13b* and *atg11-1* (Fig. 4E). In contrast, the abundance of the free-ATG8 form returned to the WT level in the complementation lines (Fig. 4F). Next, we observed and quantified ATG8a-positive autophagosomes in mesophyll protoplasts of *atg101-1*, *atg101-1* C-13, *atg101-1* C-14, and *atg13a/atg13b* lines, compared to those in the WT (Supplemental Fig. S12). The average number of fluorescent puncta was lower in *atg101-1* and *atg13a/atg13b* mutants than in the WT and *atg101-1* C-13 and *atg101-1* C-14, suggesting a reduced autophagic flux in the autophagic mutants (Supplemental Fig. S12). Collectively, these results revealed the function of ATG101; its deficiency delayed the progression of autophagy, as observed with other mutations of the ATG1 complex.

## Crossing with the *atg101-1* mutant alleviates the growth defects of the cytosolic TGP enzyme mutants

Since cytosolic TGP enzymes interact with ATG101 (Fig. 3), we crossed glycolytic enzyme mutants with the *atg101-1* mutant to determine a possible genetic relationship. Seedlings were observed for abnormality in growth under various sugar concentrations (Fig. 5A; Supplemental Fig. S11). Both WT and *atg101-1* seedlings showed normal growth in media containing 15 mM sucrose, as was also observed in *hxk1-3* and *hxk1-3 atg101-1* double mutants (Figs. 5, A and B, Supplemental Fig. S13). As shown in Fig. 2, a high percentage of TGP mutant seedlings exhibited abnormal leaves near the SAM with altered thickness and shape in 15 mM sucrose (Fig. 5B). *pgk3-2* seedlings showed a particularly high percentage of developmental defects. However, increasing sucrose concentrations (30 and 60 mM) progressively suppressed the abnormal growth of TGP mutants, including *pgk3-2* (Fig. 5A, Supplemental Fig. S13). Interestingly, crossing with the *atg101-1* mutant significantly suppressed abnormal leaf growth in these mutants under all sucrose conditions (Fig. 5A, Supplemental Fig. S13). In addition, RT-qPCR demonstrated that the expression of *SAUR15*, *EXP8*, and *PRE6*, which are cell elongation/growth-related genes under the control of auxin and brassinosteroid, was downregulated in the cytosolic TGP enzyme mutants but significantly increased upon crossing with the *atg101-1* mutant (Fig. 5C), consistent with their improved growth (Fig. 5A, Supplemental Fig. S13). Combined with the increased autophagic flux in the mutants (Fig. 2), these genetic interactions suggested that cytosolic TGP enzymes may play a role in plant autophagy, possibly by modulating the activity of the ATG1 complex. Interactions with ATG101 may contribute to the noncanonical function of TGP enzymes.

## Deficiency of ATG101 suppresses the elevated autophagic flux in the cytosolic TGP enzyme mutants

To determine whether altered autophagic flux contributes to the abnormal growth of cytosolic TGP enzyme mutants, we assessed the autophagic flux in cytosolic TGP enzyme mutants and *atg101-1*-crossed double mutants. All dark/starvation (DS) samples accumulated higher levels of ATG8-PE than light/glucose (LG) samples, indicating that two days of DS treatment could induce autophagy (Fig. 6, A and B). The ATG8-PE adduct levels were higher in the cytosolic TGP enzyme mutants *cytpi*, *pgk3-1*, *pgk3-2*, and *gapc1/2* than in the WT and *hxk1-3* mutants under LG and DS conditions, suggesting an increased autophagic flux due to the deficiency of TGP enzymes (Fig. 6, A and B), consistent with previous data (Fig. 2F, Supplemental Fig. S7). Introduction of *atg101-1* mutation suppressed the increase in ATG8-PE levels in the TGP enzyme mutants, indicating that ATG101 plays a role in increasing the autophagic flux of TGP enzyme mutants.

Next, we observed autophagosomes by visualizing GFP-ATG8a puncta in leaf mesophyll protoplasts of the WT, TGP enzyme mutants, and their *atg101-1* cross lines (Fig. 6C). The number of fluorescent puncta was higher in the cytosolic TGP enzyme mutants than in their *atg101-1* cross lines and WT (Fig. 6, C and D), which is consistent with the elevation of ATG8 lipidation in the mutants (Fig. 6, A and B). Thus, the *atg101* mutation appears to suppress the formation of ATG8-PE adducts and autophagosomal puncta in TGP enzyme mutants. Taken together, these results suggest that cytosolic TGP enzymes can modulate autophagic flux by acting upstream of the ATG1 complex, at least partly through the ATG101 interaction.

## Cytosolic TGP enzymes negatively regulate ATG1 kinase activity

Based on the genetic and biochemical relationship between cytosolic TGP enzymes and ATG101, we hypothesized that the stimulation of autophagic flux in cytosolic TGP enzyme mutants might be caused by an increase in ATG1 kinase activity. To address this hypothesis, we measured the kinase activity of ATG1 *in planta*. Plant ATG6/Beclin/Vps30 (ATG6) is a subunit of the phosphatidylinositol-3-kinase (PI3K) complex that functions downstream of the ATG1 kinase complex (Liu et al. 2005; Huang et al. 2019). Beclin, the mammalian homolog of ATG6, is a well-characterized downstream substrate of ULK1/2 (Russell et al. 2013). We performed kinase assays using immunoprecipitated YFP-ATG1a with purified recombinant MBP or MBP-ATG6 as the substrate (Supplemental Fig. S14A). We first demonstrated the autophosphorylation activity of YFP-ATG1a via autoradiography of a phosphorylated protein band of correct size (Supplemental Fig. S14B). We then examined whether YFP-ATG1a possesses transphosphorylation activity toward MBP-ATG6. The kinase assay showed that MBP-ATG6, but not MBP, was phosphorylated by YFP-ATG1a kinase, suggesting that ATG6 is a

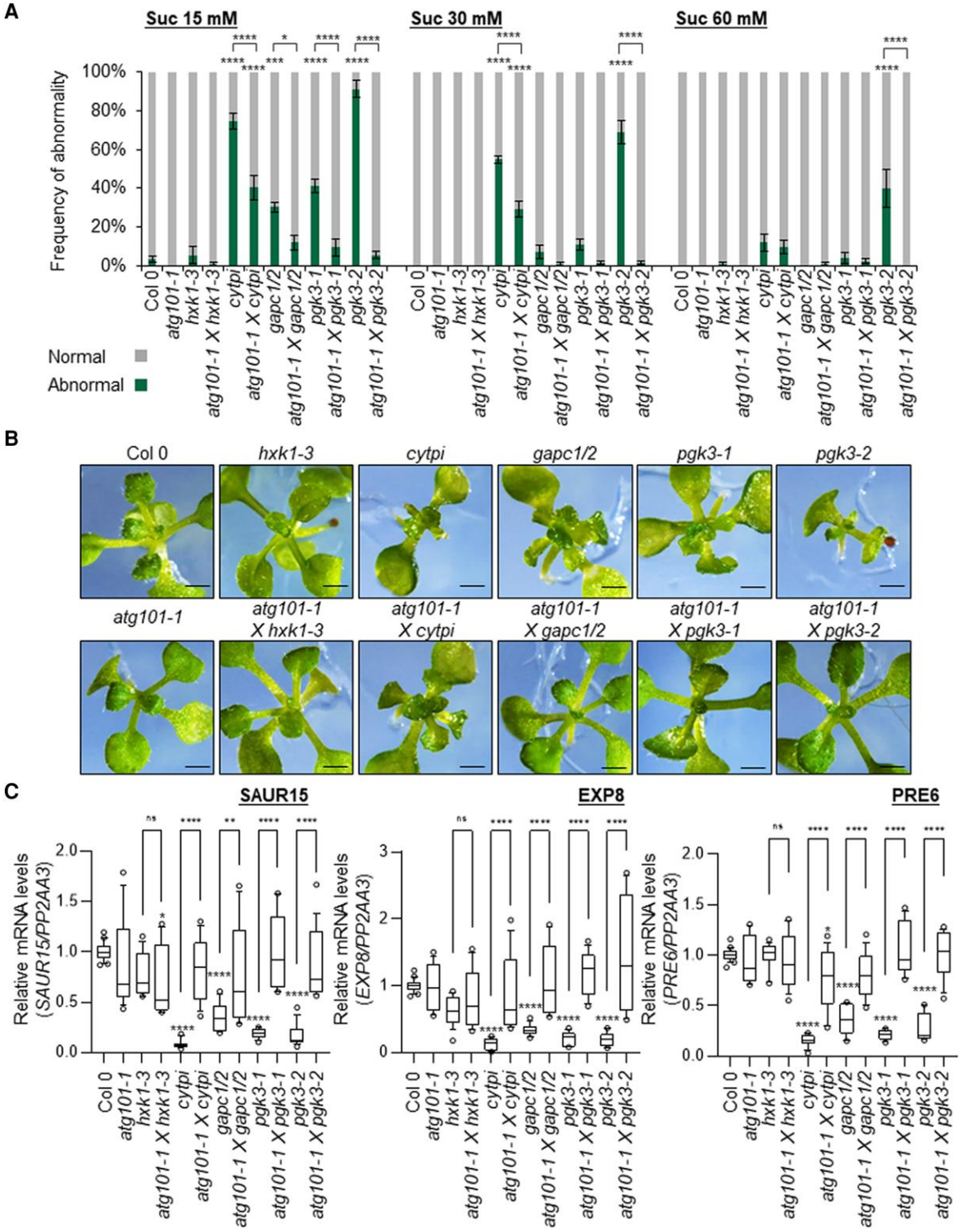


**Figure 5.** Abnormal growth phenotype of glycolytic enzyme mutants is rescued by crossing with the *atg101-1* mutant. **A)** Frequency of abnormality in the seedlings. The bar graphs show percentages of abnormal seedlings out of total 20 seedlings in 15, 30, and 60 mM sucrose. Error bars represent SE from biological replications ($n = 6$). Statistical significance was assessed using one-way ANOVA followed by Tukey's multiple comparison test (*, $P < 0.05$; ***, $P < 0.001$; ****, $P < 0.0001$). The statistical significances compared to WT (Col-0) are marked at the top of the bars, while other comparisons are indicated by respective *brackets*. **B)** Representative close-up views of the shoot apical regions of the seedlings shown in 15 mM sucrose. Scale bar = 0.2 mm. **C)** RT-qPCR analyses of cell expansion-related genes in the seedlings shown in 15 mM sucrose. The box plots represent the 1st and 3rd quartiles, centerline indicates median, represented dots are outliers, and whiskers include the 10th to 90th percentile of the data points. Statistical significance was assessed from 4 biological replications using one-way ANOVA followed by Tukey's multiple comparison test (*, $P < 0.05$; **, $P < 0.01$; ****, $P < 0.0001$).

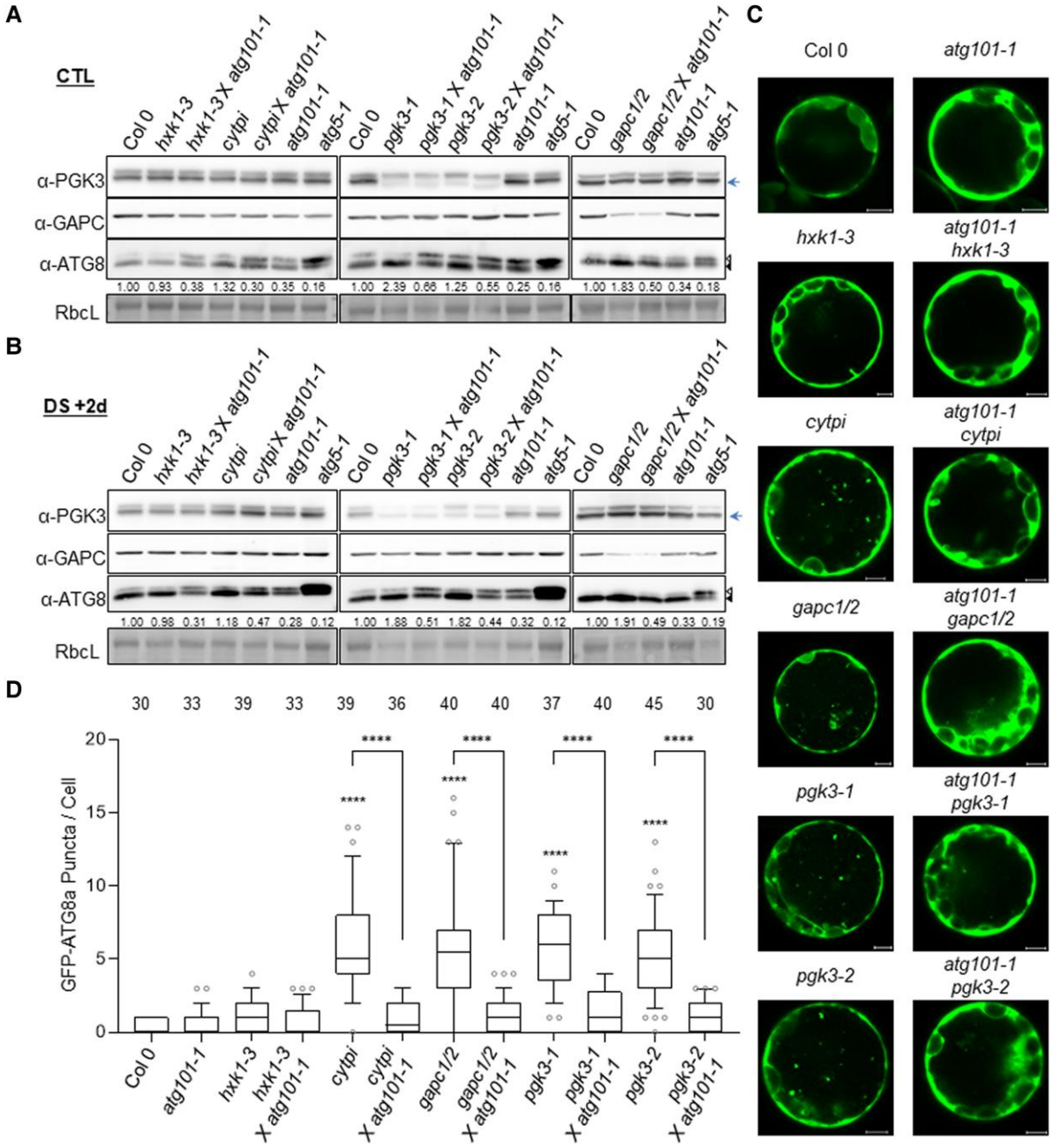


**Figure 6.** Deficiency of ATG101 suppresses increased autophagy flux in the glycolytic enzyme mutants. **A, B)** Immunoblotting to examine ATG8-PE/ATG8 patterns in the single glycolysis mutants and the double mutants (*atg101-1* cross lines). Twelve-day-old seedlings were transferred to the liquid medium containing 30 mM glucose and incubated in the light for 2 days (A; CTL) or in dark/starvation (DS) conditions for 2 days (B; DS + 2d). Then immunoblotting was performed with anti-PGK3, anti-GAPC1, and anti-ATG8 antibodies. Ponceau S-stained rubisco large subunit (rbcL) was used as the loading control. The ATG8 and ATG8-PE are marked by *open* and *closed arrowheads*, respectively. The PGK3 protein band is marked by the *arrow*. Relative band intensities of ATG8-PE/ATG8 are indicated below the anti-ATG8 image. **C)** Observation of the GFP-ATG8a fluorescence (Z-stack image projection) in the mesophyll protoplasts of single and double mutants. Leaf protoplasts were transfected with the GFP-ATG8a construct, followed by Con A (1 $\mu$M) treatment. Then, GFP-ATG8a puncta in the protoplasts were observed under a confocal microscope. Scale bars = 5 $\mu$m. **D)** The GFP-ATG8a puncta in the protoplasts were counted in Z-stacked confocal microscopy images after Con A treatment. The box plot represents the 1st and 3rd quartiles, centerline indicates median, represented dots are outliers, and whiskers include the 10th to 90th percentile of the data points. The number of biologically independent observations (*n*) is indicated on top of the graph. Statistical significance was evaluated using one-way ANOVA followed by Tukey's multiple comparison test (****, $P < 0.0001$). The statistical significances compared to WT (Col-0) are marked at the top of the bars, while other comparisons are indicated by respective *brackets*.

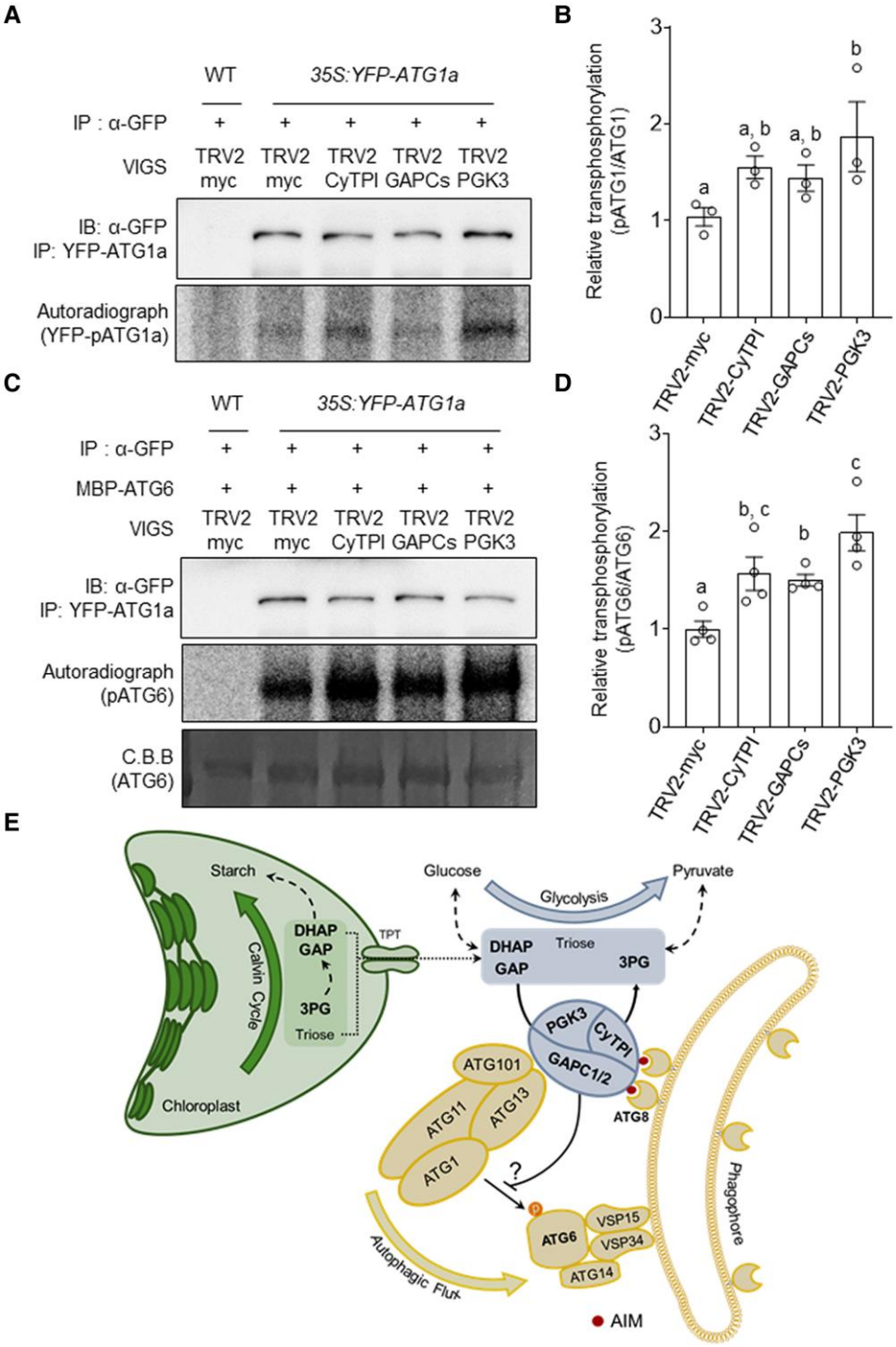


**Figure 7.** Silencing of cytosolic TGP enzymes results in increased ATG1 kinase activity. **A)** Autophosphorylation activity of ATG1a. YFP-ATG1a protein was immunoprecipitated by GFP-Trap agarose resin after VIGS of the glycolytic enzyme genes in 35Sp:YFP-ATG1a line. *In vitro* kinase assay was performed with immunoprecipitated YFP-ATG1a. The autoradiograph images indicate autophosphorylation levels of YFP-ATG1a in different VIGS plants. Immunoblotting using anti-GFP antibody showed the level of immunoprecipitated YFP-ATG1a in each sample. Three independent experiments yielded similar results and representative images are shown. **B)** Quantification for relative autophosphorylation levels of YFP-ATG8a shown in (A). Autoradiograph band intensities were divided by immunoblotting band intensities of YFP-ATG1a, and the ratio is presented relative to the TRV2-myc control. Error bars represent SE from 3 biological replications. Statistical significance was calculated by linear mixed effect modeling; letters above the boxes (*a* and *b*) indicate the results of Tukey's *post hoc* test ($P < 0.05$). **C)** Transphosphorylation activity of ATG1a toward ATG6. *In vitro* kinase assay was performed with immunoprecipitated YFP-ATG1a from VIGS plants and purified recombinant MBP-ATG6 protein.

(continued)

substrate of ATG1a in plants, findings similar to those reported in mammals (Supplemental Fig. S14, C and D). Next, to examine whether the ATG1 kinase activity is related to the autophagic flux of cytosolic TGP enzymes, we performed kinase assays using immunoprecipitated YFP-ATG1a after VIGS of TGP enzymes and control genes in *35Sp:YFP-ATG1a* line (Supplemental Fig. S14E). The TGP VIGS samples showed increased phospho-band intensity in ATG1a autophosphorylation and ATG6 phosphorylation compared to the TRV2-myc control (Fig. 7, A to D). Thus, the deficiency of cytosolic TGP enzymes stimulates the ATG1 kinase activity, subsequently increasing the autophagic flux. Taken together, these data suggest that cytosolic TGP enzymes negatively regulate autophagy by modulating the ATG1 kinase activity (Fig. 7E).

## Discussion

Nutrient availability is a weighting factor for the balance between catabolism and anabolism (Gonzalez et al. 2020). As most phototrophic organisms mainly produce energy and carbonic materials via photosynthesis, the mechanisms of autophagy regulation via carbon starvation may be different from those of heterotrophic organisms. Recent evidence suggests that plants may regulate autophagy differentially in response to carbon and nitrogen starvation (Huang et al. 2019). For example, plants induce autophagy upon nitrogen starvation only through ATG1 kinase, but in response to carbon starvation, use both ATG1-dependent and -independent mechanisms (Huang et al. 2019). These complex regulations indicate that plants may have evolved to manage autophagy more flexibly in response to carbon depletion because of their photoautotrophic nature. Plants accumulate starch during the daytime and consume it at nighttime. It has been previously proposed that autophagy may also contribute to supplying energy during nighttime or etiolation (Izumi et al. 2013; Avin-Wittenberg et al. 2015). We hypothesized that plants might have specific mechanisms for monitoring carbon availability to modulate the autophagic flux.

To address this hypothesis, we performed VIGS screening; subsequent analyses suggested that the autophagic flux is modulated by consecutive TGP enzymes (CyTPI, GAPC1/2, and PGK3) in the cytosolic glycolysis pathway (Fig. 1, A and B). Indeed, carbohydrates produced from the Calvin–Benson cycle in chloroplasts are transported to the cytosol in a triose phosphate form by a triose-phosphate/phosphate translocator (TPT) located in the chloroplast envelope (Walters et al. 2004). Structural analysis revealed that only 3rd carbon-phosphorylated trioses (i.e. DHAP, GAP, and 3-PG) and inorganic phosphate are preferentially transported by the TPT antiporter (Lee et al. 2017b). These triose phosphates, transported from chloroplasts through TPT, can become substrates of TGP enzymes in the cytosol. Moreover, these three enzymes interact with each other in the cytosol, possibly forming a protein complex (Fig. 1F, Supplemental Fig. S4). TGP interactions are also found in pull-down fractions by mitochondrial outer membrane protein, VDAC (voltage-dependent anion channel), and in pan-plant protein complex mass-spectrometry results (Graham et al. 2007; McWhite et al. 2020). Moreover, there is recent supportive evidence for forming glycolytic enzyme subcomplexes in plants. Zhang et al. (2020) suggested that a phosphoglycerate mutase and enolase form a substrate-channeling metabolon associated with pyruvate kinase. Taken together, the three TGP enzymes seemed to be located at a strategic point in the cytosolic glycolysis pathway to monitor photosynthetic efficiency by sensing the availability of their substrates (Fig. 1B, Supplemental Fig. S2).

In this study, we identified novel interactions between TGP enzymes and the ATG1 regulatory subunits ATG101 and ATG13 (Fig. 3A, Supplemental Fig. S9). Considering the upregulated ATG1a kinase activity in the TGP VIGS plants (Fig. 7), the cytosolic TGP enzymes can negatively regulate autophagy by repressing the activity of the ATG1 complex and possibly by blocking access to its downstream components. Triose phosphates transported from chloroplasts may play a role in the repression of autophagy by binding to TGP enzymes as substrates, thereby maintaining the active conformation of enzymes in the cytosol. Therefore, the interactions between cytosolic TGP enzymes and ATG101/ATG13 may connect the photosynthetic efficiency to autophagy induction. ATG101 often interacts with CyTPI and GAPCs in large foci structures in an AIM sequence-dependent manner (Fig. 3). Interestingly, the AIM sequences in CyTPI and GAPCs were highly conserved in most land plants, including ferns, lycophytes, and bryophytes (Fig. 3C). Considering that these land plants also possess all the components of the ATG1 complex, including ATG101, the mechanism of autophagy regulation by TGP enzymes may be conserved in most land plants. During the formation of early preautophagosomal structures in yeast, ATG1

**Figure 7.** (Continued)
The autoradiograph image indicates phosphorylated MBP-ATG6 by YFP-ATG1a. Coomassie Brilliant Blue (CBB) staining shows input levels of MBP-ATG6 proteins. Four independent experiments yielded similar results and representative images are shown. **D)** Quantification for relative phosphorylation levels of MBP-ATG6 shown in (C). Autoradiograph band intensities were divided by CBB-stained MBP-ATG6 intensities, and the ratio is presented relative to the TRV2-myc control. Error bars represent SE from 3 biological replications. Statistical significance was calculated by linear mixed effect modeling; letters above the boxes (*a*–*c*) indicate the results of Tukey's *post hoc* test ($P < 0.05$). **E)** A schematic model of autophagy regulation mechanisms by cytosolic TGP enzymes. The TGP enzymes (CyTPI, PGK3, and GAPC1/2) in the cytosolic glycolysis pathway, which use triose phosphates transported from chloroplasts via a TPT antiporter, play a role in autophagy regulation. The enzymes interact with ATG101 and ATG13 subunits of the ATG1 kinase complex that controls the initiation and growth of autophagosomes and suppress an increase in autophagic flux by inhibiting the ATG1 kinase activity.

complex components undergo phase separation. Phase separation of the ATG1 complex facilitates activation of ATG1 kinase activity and is negatively controlled by TOR kinase through phosphorylation of ATG13 (Fujioka et al. 2020). Although it has not been revealed that the plant ATG1 kinase activity is regulated through phase separation of the ATG1 complex, the interactions between TGP enzymes and ATG proteins could be important to modulate the phase separation processes of ATG1 complex components. Future research would reveal the underlying mechanism of how TGP enzymes affect the ATG1 kinase activity through interaction with ATG101. Collectively, our results revealed a plant-specific mechanism of autophagy regulation, which employs three consecutive triose phosphate-processing glycolytic enzymes. In addition, when our article was about to be submitted, Guan et al. (2022) reported that GAPCs and PGK3 are involved in the regulation of autophagy by heightening the inhibition of ATG3-ATG8e and ATG6-VPS34 interactions by phosphatidic acid. Thus, TGP enzymes are shown to be involved in the regulation of autophagy, responding to photosynthetic activity and the second messenger molecules, but detailed mechanisms behind these regulations remain to be uncovered.

The mutants of the TGP enzyme genes exhibited sugar-dependent abnormalities in the leaf development near shoot apical meristem (SAM) (Fig. 2). Activation of SAM relies on both light signaling and photosynthesis-driven nutrient sensing, and both pathways converge at the activation of TOR kinase (Pfeiffer et al. 2016; Li et al. 2017). Considering that the active TOR kinase firmly inhibits nutrient starvation-induced autophagy (Pu et al. 2017), the cellular state of the autophagic flux may influence stem cell maintenance/differentiation, depending on nutrient availability. Indeed, a recent study revealed that autophagy contributes to root meristem size regulation in a glucose-dependent manner (Huang et al. 2019). In potato, GAPCs are involved in controlling cold-induced sweetening and apical dominance of tubers (Liu et al. 2017). Potato GAPCs interact with ATG3, suggesting that the occurrence of cell death in tuber apical bud meristems could be induced by autophagy through interaction with ATG3 (Liu et al. 2017). Furthermore, cell elongation is regulated by the stability of BRASSINAZOLE RESISTANT 1 (BZR1) and BRI-EMS SUPPRESSOR1 (BES1) transcription factors via selective autophagy (Nolan et al. 2017; Yang et al. 2017). BZR1 and BES1 are ubiquitinated and docked in the autophagic body via DOMINANT SUPPRESSOR OF KAR2 (DSK2), an autophagic adaptor protein (Nolan et al. 2017). Moreover, BZR1/BES1-related selective autophagy is modulated by the TOR pathway, which controls cell elongation according to nutrient availability (Zhang et al. 2016). Accordingly, the cell division/elongation defects of the cytosolic TGP enzyme mutants at low sucrose concentrations (Fig. 2) may be related to the uncontrolled degradation of unidentified target proteins via increased autophagic flux. Indeed, the leaf developmental defect of the TGP mutants was alleviated upon crossing with *atg101-1* or increasing sugar concentrations (Fig. 5). The *atg101-1* mutant exhibited typical autophagy-deficient phenotypes, similar to other subunits of the ATG1 complex (Fig. 4). Taken together, our results suggest that CyTPI, GAPCs, and PGK3 not only regulate autophagy, acting epistatically upstream of the ATG1 complex but may also coordinate cell division/elongation through autophagy regulation. Identifying further interacting partners of CyTPI, GAPCs, and PGK3 may help explain how plants modulate growth via autophagy according to nutrient availability.

## Materials and methods

### Plant materials and growth conditions

All the seed information is described in Supplemental Table S1. Briefly, *35Sp:GFP-ATG8a* and *atg13a/atg13b* lines were kindly provided by Dr. Taijoon Chung (Pusan University, Korea) and Dr. Faqiang Li (South China Agricultural University, China), respectively. All T-DNA insertion mutant lines were obtained from the Arabidopsis Biological Resource Center. The double mutants *hxk1-3* × *atg101-1*, *cytpi* × *atg101-1*, *gapc1/2* × *atg101-1*, *pgk3-1* × *atg101-1*, and *pgk3-2* × *atg101-1* were generated by crossing between the mutants, and T3 homozygous seeds were used in this study. Complementation lines for *atg101-1* were generated using pCAMBIA-ATG101p(-628 bp):YFP-ATG101 construct via *Agrobacterium tumefaciens*-mediated transformation, and two independent T3 homozygous lines (C13 and C14) were used in this study.

For VIGS and transient expression, Arabidopsis (*Arabidopsis thaliana*) and *N. benthamiana* plants were grown in soil in a growth chamber (22 °C, 60% humidity, 100 to 120 $\mu$mol $m^{-2}$ $s^{-1}$ light intensity using light bulbs [Philips TLD36W/865/FL40SS/36/EX-D], and 16-h-light/8-h-dark cycle). For the liquid culture, *Arabidopsis* seeds were surface-sterilized with 70% (v/v) ethanol, incubated at 4 °C for 1 day for stratification, and then sown in 6-well or 12-well plates containing 1 or 0.5 mL of liquid medium (1/2 MS basal salt medium [Duchefa, M0221], pH 5.7 adjusted by KOH), respectively. After germination, seedlings were grown in 1/2 MS liquid medium containing 30 mM glucose, which was changed every other day. For the analysis of growth phenotype, *Arabidopsis* seeds were surface-sterilized and imbibed and then grown in plates (1/2 MS basal salts, pH 5.7 adjusted by MES-KOH, and 0.6% (w/v) phytoagar [Duchefa, P1001]) containing various sugar concentrations.

### Virus-induced gene silencing

Target gene sequences of *AtTOR* complex genes and 45 metabolic genes (Supplemental Table S2) were amplified by PCR with gene-specific primers (Supplemental Table S3) and then cloned into pTRV2 vector (Burch-Smith et al. 2006) using In-Fusion cloning (Takara) (Supplemental Table S4). Both pTRV1 and pTRV2 vectors were introduced into *A. tumefaciens* (GV3101 strain). pTRV2-Myc was used as a negative control for VIGS. VIGS was performed in

*Arabidopsis* as described previously (Lee et al. 2017a), using soil-grown seedlings at two to four true-leaf stages. For VIGS, we used the constructs containing 265, 330, 567, 591, and 500 bp cDNA sequences of *HXK1*, *CyTPI*, *PGK3*, *GAPC1*, and *GAPC2*, respectively.

## Visualization of phagosomes

Leaves from VIGS plants were observed by a fluorescence microscope (Olympus, BX51) and a confocal laser scanning microscope (Carl Zeiss, LSM 880) for initial screening and Z-stacked image processing (Maximum Intensity Z-projection), respectively. Puncta numbers were counted by Fiji software.

## Bimolecular fluorescence complementation

BiFC was performed using the multicolor bimolecular fluorescence complementation system, as previously described (Gehl et al. 2009). Coding sequences (CDSs) of *HXK1*, *CyTPI*, *GAPC1*, *GAPC2*, *PGK3*, *ATG101*, *ATG13A*, *ATG13B*, *PdTPI*, *PGK2*, and *PGK3* were cloned into Fu79 entry vector (Wang et al. 2013) or Fu79$^{Inv}$ entry vector (without stop codon) by Infusion cloning (Supplemental Table S4). AIM motif mutated *CyTPI* $^{mAIM}$ and *GAPC1*$^{mAIM}$ was generated by site-directed mutagenesis (Supplemental Table S3). All entry vectors were used for subcloning into destination vectors as indicated in Supplemental Table S4 (ThermoFisher Scientific, 11791100). *Agrobacterium tumefaciens* GV3101 strains containing the VYNE (and/or SCYNE), VYCE (and/or SCYCE), and 35Sp:p19 construct were coinfiltrated at the adjusted $OD_{600}$ as 0.7:0.7:1 into leaves of 3-week-old *N. benthamiana* plants. BiFC signals were monitored 36 to 48 h after infiltration in the abaxial side of the leaf epidermis using a confocal laser scanning microscope (Carl Zeiss, LSM 700). To combine colocalization and BiFC, *A. tumefaciens* GV3101 strains containing SCYNE, SCYCE, pCAMBIA1390-35Sp:mCherry-ATG8a, and 35S:p19 constructs were coinfiltrated at the adjusted $OD_{600}$ as 0.7:0.7:0.2:1 into leaves of *N. benthamiana* plants.

## Reverse transcription quantitative PCR

Total RNA was extracted using the IQeasy Plus Plant RNA Extraction Mini kit (iNtRON Biotechnology; Korea) according to the manufacturer's instructions. The cDNA synthesis was performed with 1 $\mu$g of total RNA using the RevertAid First Standard cDNA synthesis kit (ThermoFisher Scientific, K1622) and oligo(dT) primers, according to the manufacturer's instructions. RT-qPCR was performed in a 96-well plate using diluted cDNAs (1:100), RealHelix qPCR kit (NANOHELIX; Korea), and the StepOnePlus Realtime PCR System (Applied Biosystems, 4376600) with specific primer sets (Supplemental Table S3). Normalization was performed as described in the figure legends, using *PP2AA3* (AT1G13320) mRNA as a reference gene.

## Immunoblotting for ATG8/ATG8-PE detection

To measure the autophagic flux, immunoblotting was performed with 12-day-old seedlings grown in the liquid culture. Homogenized samples were resuspended in the same volume of the protein extraction buffer (50 mM Tris-HCl pH 7.5, 150 mM NaCl, 1% (v/v) NP-40, 0.1% (w/v) SDS, 0.5% (w/v) sodium deoxycholate, 2 mM $Na_3VO_4$, 2 mM NaF, 20 mM β-glycerophosphate, and complete protease inhibitor cocktail [Roche, 11836170001]). After centrifugation, NuPAGE LDS sample buffer (ThermoFisher Scientific, NP0007) was added for incubation at 70 °C for 10 min. Twenty-five micrograms of total protein was subjected to cooled SDS-PAGE (4% to 20% gradient gel) with low voltage (100 V). The gel was divided into upper (>30 kDa) and lower (<30 kDa) parts and then separately transferred to 0.45 and 0.20 $\mu$m pore-size polyvinylidene difluoride membranes, respectively. Immunoblotting was performed with the rabbit polyclonal anti-ATG8 (Agrisera, AS14 2769; 1:5,000), anti-GAPC1/2 (Agrisera, AS15 2894; 1:10,000), and anti-PGK3 (produced from rabbits by repeated injection using recombinant His-PGK3 protein; 1:10,000, GW Vitek, Korea) antibodies and mouse monoclonal anti-GFP antibody (Roche, 11814460001; 1:5,000). Signals were detected by Imagequant LAS 4000 (GE Healthcare).

## Protoplast isolation and transfection

*Arabidopsis* mesophyll protoplasts were isolated, as described previously (Yoo et al. 2007). Briefly, leaves from 4-week-old *Arabidopsis* plants (grown in 16 h light/8 h dark) were cut into strips and then incubated in the digestion solution (20 mM MES-KOH pH 5.7, 1.5% (w/v) Cellulase R-10 [Yakult; Japan], 0.4% (w/v) Macerozyme R-10 [Yakult; Japan], 0.4 M mannitol, 20 mM KCl, 10 mM $CaCl_2$, and 0.1% (w/v) BSA) for 3 h in the dark. The protoplasts were washed using W5 buffer (2 mM MES-KOH pH 5.7, 154 mM NaCl, 125 mM $CaCl_2$, and 5 mM KCl) and collected by centrifugation at 100 *g* for 2 min. For autophagosome observation, protoplasts ($10^5$ cells) were transfected with 10 $\mu$g of p326-sGFP-ATG8a plasmid DNA for 16 h in WI solution (4 mM MES-KOH pH 5.7, 0.5 M mannitol, and 20 mM KCl). For Concanmycin A (APExBio, A8633) treatment, 1 $\mu$M Con A was treated for 16 h along with transfection.

## *In vitro* kinase assay using immunoprecipitated ATG1a

The full length of ATG6 CDS was cloned into the pMal-C2X vector for MBP fusion using infusion cloning (Takara). The constructs were transformed into *Escherichia coli* BL21 (DE3) strain. MBP-fusion proteins were expressed by 0.25 mM Isopropyl-β-D-thiogalactopyranosid treatment at 37 °C to an $OD_{600}$ of 0.4 and purified using Amylose resin (New England Biolabs, E8021), following the manufacturer's instruction with a purification buffer (20 mM Tris-HCl and 200 mM NaCl). After purification, proteins were concentrated using Amicon Ultracel 30 K (Merck, UFC503096) according to the manufacturer's instructions.

Kinase assay was performed as previously described with minor modifications (Sanchez-Wandelmer et al. 2017).

YFP-ATG1a protein was expressed in *N. benthamiana* leaves or *Arabidopsis* stable transgenic line (35Sp:YFP-ATG1a). Total proteins were extracted in buffer A (100 mM Tris-HCl, pH 7.5, 300 mM NaCl, 10 mM EDTA, 10 mM EGTA, 1% (v/v) NP-40, 10 mM $Na_3VO_4$, 10 mM NaF, 1 mM phenylmethylsulfonylfluoride, 10% (v/v) glycerol, and protease inhibitor cocktail [Roche, 11836170001]). YFP-ATG1a proteins were collected by GFP-Trap agarose resin (Chromotek, gta-10) for 4 h at 4 °C and washed 4 times with buffer A without glycerol, followed by washing twice with buffer B (20 mM MOPS, pH 7.5, 1 mM EGTA, 10 mM $Na_3VO_4$, and 15 mM $MgCl_2$). Kinase assay was performed with 2 μCi [$\gamma$-$^{32}$P]-ATP, immunoprecipitated YFP-ATG1a, and 5 $\mu$g recombinant substrate proteins in 20 $\mu$L buffer B for 20 min at 30 °C. After subjecting SDS-PAGE, the gel was stained and then dried using a gel dryer. Radioactivity was detected using a phosphorimager (BAS-2500, Fujifilm). Immunoblotting of immunoprecipitated YFP-ATG1a was performed with the anti-GFP antibody (Roche, 11814460001).

### Statistical analysis

GraphPad PRISM 9.0 and R & Bioconductor (Ver. 4.1.2) were used for most data analyses and visualization. Outliers were determined and removed using the ROUT test, performed in GraphPad PRISM. Two-sided unpaired *t*-test and one-way ANOVA were implemented in GraphPad PRISM and R & Bioconductor. *Post hoc* tests following the ANOVA were specified in the figure legends.

### Accession numbers

Sequence data from this article can be found in the GenBank/EMBL data libraries under accession numbers: AT3G55440 (CyTPI), AT3G04120 (GAPC1), AT1G13440 (GAPC2), AT1G79550 (PGK3), and AT5G66930 (ATG101). The accession numbers of all genes used in this study are listed in Supplemental Table S2.

## Acknowledgments

We thank Dr. Taijoon Chung (Pusan National University) and Tae-Wuk Kim (Hanyang University) for helpful discussions. We are grateful to Dr. Faqiang Li (South China Agricultural University), Dr. Taijoon Chung, and Dr. Richard D. Vierstra (Wisconsin University) for generously providing the seeds of *35Sp:GFP-ATG8a* and *atg13a-1/atg13b-2*.

## Author contributions

D.-H.L. and H.-S.P. conceived, designed, and coordinated the project. D.-H.L. and I.C. performed all the experimental works with S.J.P. and S.K. D.-H.L., I.C., M.-S.C., H.-S.L. and H.-S.P. analyzed the results. D.-H.L. and H.-S.P. wrote the manuscript. D.-H.L. and I.C. contributed equally. All authors discussed the results and commented on the manuscript.

## Supplemental data

The following materials are available in the online version of this article.

**Supplemental Figure S1.** A proof of concept for VIGS screening to identify autophagy-modulating genes.

**Supplemental Figure S2.** Schematic representation of the glycolysis- and Calvin–Benson cycle-related enzymes selected for VIGS screening.

**Supplemental Figure S3.** VIGS phenotypes and RT-qPCR analyses to measure reduced mRNA levels.

**Supplemental Figure S4.** Cytosolic TGP enzymes interact with each other.

**Supplemental Figure S5.** Analyses of the T-DNA mutants of the glycolysis enzymes.

**Supplemental Figure S6.** Growth phenotypes of the T-DNA mutants at different sucrose concentrations.

**Supplemental Figure S7.** Immunoblotting for monitoring ATG8-PE/ATG8 patterns.

**Supplemental Figure S8.** Immunoblotting to check expression for Fig. 3A.

**Supplemental Figure S9.** The cytosolic TGP enzymes interact with ATG13 and ATG101.

**Supplemental Figure S10.** Coimmunoprecipitation to examine ATG8 interactions with the glycolytic enzymes and their mutants (mAIM).

**Supplemental Figure S11.** Genotyping for *atg101-1* mutant.

**Supplemental Figure S12.** *atg101-1* showed less GFP-ATG8a puncta than WT and its complemented lines.

**Supplemental Figure S13.** Abnormal phenotypes of the glycolysis mutants were alleviated by crossing with *atg101-1* mutant.

**Supplemental Figure S14.** ATG1a kinase phosphorylates ATG6 *in vitro*.

**Supplemental Methods.** Additional methods.

**Supplemental Table S1.** List of genotypes used in this study

**Supplemental Table S2.** List of genes used in this study

**Supplemental Table S3.** List of primers used in this study

**Supplemental Table S4.** List of constructs used in this study

## Funding

This research was supported by the National Research Foundation of Korea (NRF-2018R1A6A1A03025607; Basic Science Research Program | NRF-2022R1A2C1009088; Mid-Career Researcher Program). D.-H.L. was supported by Yonsei University (Brain Korea 21 Fellowship).

*Conflict of interest statement.* The authors declare that they have no conflict of interests.

## Data availability

All data supporting the findings of this study are available from the corresponding authors upon request.

## References


**Avin-Wittenberg T, Bajdzienko K, Wittenberg G, Alseekh S, Tohge T, Bock R, Giavalisco P, Fernie AR**. Global analysis of the role of autophagy in cellular metabolism and energy homeostasis in Arabidopsis seedlings under carbon starvation. Plant Cell. 2015:**27**(2):306–322. https://doi.org/10.1105/tpc.114.134205

**Burch-Smith TM, Schiff M, Liu Y, Dinesh-Kumar SP**. Efficient virus-induced gene silencing in Arabidopsis. Plant Physiol. 2006:**142**(1):21–27. https://doi.org/10.1104/pp.106.084624

**Chen L, Su ZZ, Huang L, Xia FN, Qi H, Xie LJ, Xiao S, Chen QF**. The AMP-activated protein kinase KIN10 is involved in the regulation of autophagy in Arabidopsis. Front Plant Sci. 2017:**8**:1201. https://doi.org/10.3389/fpls.2017.01201

**Chen M, Thelen JJ**. The plastid isoform of triose phosphate isomerase is required for the postgerminative transition from heterotrophic to autotrophic growth in Arabidopsis. Plant Cell. 2010:**22**(1):77–90. https://doi.org/10.1105/tpc.109.071837

**Cho YH, Yoo SD, Sheen J**. Regulatory functions of nuclear hexokinase1 complex in glucose signaling. Cell. 2006:**127**(3):579–589. https://doi.org/10.1016/j.cell.2006.09.028

**Chung T, Phillips AR, Vierstra RD**. ATG8 Lipidation and ATG8-mediated autophagy in Arabidopsis require ATG12 expressed from the differentially controlled ATG12A AND ATG12B loci. Plant J. 2010:**62**(3):483–493. https://doi.org/10.1111/j.1365-313X.2010.04166.x

**Dettmer J, Hong-Hermesdorf A, Stierhof YD, Schumacher K**. Vacuolar H+-ATPase activity is required for endocytic and secretory trafficking in Arabidopsis. Plant Cell. 2006:**18**(3):715–730. https://doi.org/10.1105/tpc.105.037978

**Fujioka Y, Alam JM, Noshiro D, Mouri K, Ando T, Okada Y, May AI, Knorr RL, Suzuki K, Ohsumi Y, et al.** Phase separation organizes the site of autophagosome formation. Nature. 2020:**578**(7794):301–305. https://doi.org/10.1038/s41586-020-1977-6

**Gehl C, Waadt R, Kudla J, Mendel RR, Hänsch R**. New GATEWAY vectors for high throughput analyses of protein-protein interactions by bimolecular fluorescence complementation. Mol Plant. 2009:**2**(5):1051–1058. https://doi.org/10.1093/mp/ssp040

**Gonzalez A, Hall MN, Lin SC, Hardie DG**. AMPK and TOR: the yin and yang of cellular nutrient sensing and growth control. Cell Metab. 2020:**31**(3):472–492. https://doi.org/10.1016/j.cmet.2020.01.015

**Graham JWA, Williams TCR, Morgan M, Fernie AR, Ratcliffe RG, Sweetlove LJ**. Glycolytic enzymes associate dynamically with mitochondria in response to respiratory demand and support substrate channeling. Plant Cell. 2007:**19**(11):3723–3738. https://doi.org/10.1105/tpc.107.053371

**Guan B, Jiang YT, Lin DL, Lin WH, Xue HW**. Phosphatidic acid suppresses autophagy through competitive inhibition by binding GAPC (glyceraldehyde-3-phosphate dehydrogenase) and PGK (phosphoglycerate kinase) proteins. Autophagy. 2022:**18**(11):2656–2670. https://doi.org/10.1080/15548627.2022.2046449

**Han S, Wang Y, Zheng X, Jia Q, Zhao J, Bai F, Hong Y, Liu Y**. Cytoplastic glyceraldehyde-3-phosphate dehydrogenases interact with ATG3 to negatively regulate autophagy and immunity in Nicotiana benthamiana. Plant Cell. 2015:**27**(4):1316–1331. https://doi.org/10.1105/tpc.114.134692

**Henry E, Fung N, Liu J, Drakakaki G, Coaker G**. Beyond glycolysis: gAPDHs are multi-functional enzymes involved in regulation of ROS, autophagy, and plant immune responses. PLoS Genet. 2015:**11**(4):e1005199. https://doi.org/10.1371/journal.pgen.1005199

**Huang X, Zheng C, Liu F, Yang C, Zheng P, Lu X, Tian J, Chung T, Otegui MS, Xiao S, et al.** Genetic analyses of the Arabidopsis ATG1 kinase Complex reveal both kinase-dependent and independent autophagic routes during fixed-carbon starvation. Plant Cell. 2019:**31**(12):2973–2995. https://doi.org/10.1105/tpc.19.00066

**Izumi M, Hidema J, Makino A, Ishida H**. Autophagy contributes to nighttime energy availability for growth in Arabidopsis. Plant Physiol. 2013:**161**(4):1682–1693. https://doi.org/10.1104/pp.113.215632

**Jia M, Liu X, Xue H, Wu Y, Shi L, Wang R, Chen Y, Xu N, Zhao J, Shao J, et al.** Noncanonical ATG8-ABS3 interaction controls senescence in plants. Nat Plants. 2019:**5**(2):212–224. https://doi.org/10.1038/s41477-018-0348-x

**Kim SC, Guo L, Wang X**. Nuclear moonlighting of cytosolic glyceraldehyde-3-phosphate dehydrogenase regulates Arabidopsis response to heat stress. Nat Commun. 2020:**11**(1):3439. https://doi.org/10.1038/s41467-020-17311-4

**Lee Y, Nishizawa T, Takemoto M, Kumazaki K, Yamashita K, Hirata K, Minoda A, Nagatoishi S, Tsumoto K, Ishitani R, et al.** Structure of the triose-phosphate/phosphate translocator reveals the basis of substrate specificity. Nat Plants. 2017b:**3**(10):825–832. https://doi.org/10.1038/s41477-017-0022-8

**Lee DH, Park SJ, Ahn CS, Pai HS**. MRF Family genes are involved in translation control, especially under energy-deficient conditions, and their expression and functions are modulated by the TOR signaling pathway. Plant Cell. 2017a:**29**(11):2895–2920. https://doi.org/10.1105/tpc.17.00563

**Li F, Chung T, Vierstra RD**. AUTOPHAGY-RELATED11 plays a critical role in general autophagy- and senescence-induced mitophagy in Arabidopsis. Plant Cell. 2014:**26**(2):788–807. https://doi.org/10.1105/tpc.113.120014

**Li F, Vierstra RD**. Autophagy: a multifaceted intracellular system for bulk and selective recycling. Trends Plant Sci. 2012:**17**(9):526–537. https://doi.org/10.1016/j.tplants.2012.05.006

**Li L, Lee CP, Ding X, Qin Y, Wijerathna-Yapa A, Broda M, Otegui MS, Millar AH**. Defects in autophagy lead to selective in vivo changes in turnover of cytosolic and organelle proteins in Arabidopsis. Plant Cell. 2022:**34**(10):3936–3960. https://doi.org/10.1093/plcell/koac185

**Li X, Cai W, Liu Y, Li H, Fu L, Liu Z, Xu L, Liu H, Xu T, Xiong Y**. Differential TOR activation and cell proliferation in Arabidopsis root and shoot apexes. Proc Natl Acad Sci U S A. 2017:**114**(10):2765–2770. https://doi.org/10.1073/pnas.1618782114

**Liu T, Fang H, Liu J, Reid S, Hou J, Zhou T, Tian Z, Song B, Xie C**. Cytosolic glyceraldehyde-3-phosphate dehydrogenases play crucial roles in controlling cold-induced sweetening and apical dominance of potato (Solanum tuberosum L.) tubers. Plant Cell Environ. 2017:**40**(12):3043–3054. https://doi.org/10.1111/pce.13073

**Liu Y, Bassham DC**. TOR is a negative regulator of autophagy in Arabidopsis thaliana. PLoS One. 2010:**5**(7):e11883. https://doi.org/10.1371/journal.pone.0011883

**Liu Y, Schiff M, Czymmek K, Talloczy Z, Levine B, Dinesh-Kumar SP**. Autophagy regulates programmed cell death during the plant innate immune response. Cell. 2005:**121**(4):567–577. https://doi.org/10.1016/j.cell.2005.03.007

**Loos B, du Toit A, Hofmeyr JH**. Defining and measuring autophagosome flux-concept and reality. Autophagy. 2014:**10**(11):2087–2096. https://doi.org/10.4161/15548627.2014.973338

**Marshall RS, Hua Z, Mali S, McLoughlin F, Vierstra RD**. ATG8-Binding UIM proteins define a new class of autophagy adaptors and receptors. Cell. 2019:**177**(3):766–781 e724. https://doi.org/10.1016/j.cell.2019.02.009

**Masclaux-Daubresse C, Clément G, Anne P, Routaboul JM, Guiboileau A, Soulay F, Shirasu K, Yoshimoto K**. Stitching together the multiple dimensions of autophagy using metabolomics and transcriptomics reveals impacts on metabolism, development, and plant responses to the environment in Arabidopsis. Plant Cell. 2014:**26**(5):1857–1877. https://doi.org/10.1105/tpc.114.124677

**McWhite CD, Papoulas O, Drew K, Cox RM, June V, Dong OX, Kwon T, Wan C, Salmi ML, Roux SJ, et al.** A pan-plant protein complex map reveals deep conservation and novel assemblies. Cell. 2020:**181**(2):460–474 e414. https://doi.org/10.1016/j.cell.2020.02.049

**Menard L, Maughan D, Vigoreaux J**. The structural and functional coordination of glycolytic enzymes in muscle: evidence of a metabolon?

Biology (Basel). 2014:**3**(3):623–644. https://doi.org/10.3390/biology3030623

**Michaeli S, Galili G, Genschik P, Fernie AR, Avin-Wittenberg T**. Autophagy in plants—What's new on the menu? Trends Plant Sci. 2016:**21**(2):134–144. https://doi.org/10.1016/j.tplants.2015.10.008

**Mizushima N, Yoshimori T**. How to interpret LC3 immunoblotting. Autophagy. 2007:**3**(6):542–545. https://doi.org/10.4161/auto.4600

**Mizushima N, Yoshimori T, Levine B**. Methods in mammalian autophagy research. Cell. 2010:**140**(3):313–326. https://doi.org/10.1016/j.cell.2010.01.028

**Nolan TM, Brennan B, Yang M, Chen J, Zhang M, Li Z, Wang X, Bassham DC, Walley J, Yin Y**. Selective autophagy of BES1 mediated by DSK2 balances plant growth and survival. Dev Cell. 2017:**41**(1):33–46 e37. https://doi.org/10.1016/j.devcel.2017.03.013

**Pfeiffer A, Janocha D, Dong Y, Medzihradszky A, Schone S, Daum G, Suzaki T, Forner J, Langenecker T, Rempel E, et al.** Integration of light and metabolic signals for stem cell activation at the shoot apical meristem. Elife. 2016:**5**:e17023. https://doi.org/10.7554/eLife.17023

**Plaxton WC**. The organization and regulation of plant glycolysis. Annu Rev Plant Physiol Plant Mol Biol. 1996:**47**(1):185–214. https://doi.org/10.1146/annurev.arplant.47.1.185

**Pu Y, Luo X, Bassham DC**. TOR-dependent and -independent pathways regulate autophagy in Arabidopsis thaliana. Front Plant Sci. 2017:**8**:1204. https://doi.org/10.3389/fpls.2017.01204

**Qian X, Li X, Cai Q, Zhang C, Yu Q, Jiang Y, Lee JH, Hawke D, Wang Y, Xia Y, et al.** Phosphoglycerate kinase 1 phosphorylates beclin1 to induce autophagy. Mol Cell. 2017:**65**(5):917–931 e916. https://doi.org/10.1016/j.molcel.2017.01.027

**Reis M, Alves CN, Lameira J, Tuñón I, Marti S, Moliner V**. The catalytic mechanism of glyceraldehyde 3-phosphate dehydrogenase from trypanosoma cruzi elucidated via the QM/MM approach. Phys Chem Chem Phys. 2013:**15**(11):3772–3785. https://doi.org/10.1039/c3cp43968b

**Rosa-Tellez S, Anoman AD, Flores-Tornero M, Toujani W, Alseek S, Fernie AR, Nebauer SG, Muñoz-Bertomeu J, Segura J, Ros R**. Phosphoglycerate kinases are co-regulated to adjust metabolism and to optimize growth. Plant Physiol. 2018:**176**(2):1182–1198. https://doi.org/10.1104/pp.17.01227

**Russell RC, Tian Y, Yuan H, Park HW, Chang YY, Kim J, Kim H, Neufeld TP, Dillin A, Guan KL**. ULK1 induces autophagy by phosphorylating beclin-1 and activating VPS34 lipid kinase. Nat Cell Biol. 2013:**15**(7):741–750. https://doi.org/10.1038/ncb2757

**Russell RC, Yuan HX, Guan KL**. Autophagy regulation by nutrient signaling. Cell Res. 2014:**24**(1):42–57. https://doi.org/10.1038/cr.2013.166

**Sanchez-Wandelmer J, Kriegenburg F, Rohringer S, Schuschnig M, Gómez-Sanchez R, Zens B, Abreu S, Hardenberg R, Hollenstein D, Gao J, et al.** Atg4 proteolytic activity can be inhibited by atg1 phosphorylation. Nat Commun. 2017:**8**(1):295. https://doi.org/10.1038/s41467-017-00302-3

**Suttangkakul A, Li F, Chung T, Vierstra RD**. The ATG1/ATG13 protein kinase complex is both a regulator and a target of autophagic recycling in Arabidopsis. Plant Cell. 2011:**23**(10):3761–3779. https://doi.org/10.1105/tpc.111.090993

**Thompson AR, Doelling JH, Suttangkakul A, Vierstra RD**. Autophagic nutrient recycling in Arabidopsis directed by the ATG8 and ATG12 conjugation pathways. Plant Physiol. 2005:**138**(4):2097–2110. https://doi.org/10.1104/pp.105.060673

**Walters RG, Ibrahim DG, Horton P, Kruger NJ**. A mutant of Arabidopsis lacking the triose-phosphate/phosphate translocator reveals metabolic regulation of starch breakdown in the light. Plant Physiol. 2004:**135**(2):891–906. https://doi.org/10.1104/pp.104.040469

**Wang X, Fan C, Zhang X, Zhu J, Fu YF**. Biovector, a flexible system for gene specific-expression in plants. BMC Plant Biol. 2013:**13**(1):198. https://doi.org/10.1186/1471-2229-13-198

**Yang M, Li C, Cai Z, Hu Y, Nolan T, Yu F, Yin Y, Xie Q, Tang G, Wang X**. SINAT E3 ligases control the light-mediated stability of the brassinosteroid-activated transcription factor BES1 in Arabidopsis. Dev Cell. 2017:**41**(1):47–58 e44. https://doi.org/10.1016/j.devcel.2017.03.014

**Yoo SD, Cho YH, Sheen J**. Arabidopsis mesophyll protoplasts: a versatile cell system for transient gene expression analysis. Nat Protoc. 2007:**2**(7):1565–1572. https://doi.org/10.1038/nprot.2007.199

**Zhang CS, Hawley SA, Zong Y, Li M, Wang Z, Gray A, Ma T, Cui J, Feng JW, Zhu M, et al.** Fructose-1,6-bisphosphate and aldolase mediate glucose sensing by AMPK. Nature. 2017:**548**(7665):112–116. https://doi.org/10.1038/nature23275

**Zhang Y, Sampathkumar A, Kerber SM-L, Swart C, Hille C, Seerangan K, Graf A, Sweetlove L, Fernie AR**. A moonlighting role for enzymes of glycolysis in the co-localization of mitochondria and chloroplasts. Nat Commun. 2020:**11**(1):4509. https://doi.org/10.1038/s41467-020-18234-w

**Zhang Z, Zhu JY, Roh J, Marchive C, Kim SK, Meyer C, Sun Y, Wang W, Wang ZY**. TOR signaling promotes accumulation of BZR1 to balance growth with carbon availability in Arabidopsis. Curr Biol. 2016:**26**(14):1854–1860. https://doi.org/10.1016/j.cub.2016.05.005

**Zhuang X, Chung KP, Luo M, Jiang L**. Autophagosome biogenesis and the endoplasmic Reticulum: a plant perspective. Trends Plant Sci. 2018:**23**(8):677–692. https://doi.org/10.1016/j.tplants.2018.05.002